Clim. Past Discuss., https://doi.org/10.5194/cp-2018-149
Manuscript under review for journal Clim. Past
Discussion started: 14 December 2018

Climate of the Past Discussions

Simulating the Climate Response to Atmospheric Oxygen Variability in the Phanerozoic

David C. Wade[1], Nathan Luke Abraham[1,2], Alexander Farnsworth[3], Paul J. Valdes[3], Fran Bragg[3], and Alexander T. Archibald[1,2]

[1]Centre for Atmospheric Science, Department of Chemistry, Cambridge, UK
[2]National Centre for Atmospheric Science, Department of Chemistry, Cambridge, UK
[3]School of Geographical Sciences, University of Bristol, Bristol, UK

Correspondence: dcw32.wade@gmail.com, ata27@cam.ac.uk

Abstract. The amount of dioxygen (O_2) in the atmosphere may have varied from as little as 10 % to as high as 35 % during the Phanerozoic eon (541 Ma – Present). These changes in the amount of O_2 are large enough to have lead to changes in atmospheric mass, which may alter the radiative budget of the atmosphere, leading to this mechanism being invoked to explain discrepancies between climate model simulations and proxy reconstructions of past climates. Here we present the first fully 3D numerical model simulations to investigate the climate impacts of changes in O_2 during different climate states using the HadGEM3-AO and HadCM3-BL models. We show that simulations with an increase in O_2 content result in increased global mean surface air temperature under conditions of a pre-industrial Holocene climate state, in agreement with idealised 1D and 2D modeling studies. We demonstrate the mechanism behind the warming is complex and involves trade-off between a number of factors. Increasing atmospheric O_2 leads to a reduction in incident shortwave radiation at Earth's surface due to Rayleigh scattering, a cooling effect. However, there is a competing warming effect due to an increase in the pressure broadening of greenhouse gas absorption lines and dynamical feedbacks, which alter the meridional heat transport of the ocean, warming polar regions and cooling tropical regions.

Case studies from past climates are investigated using HadCM3-BL which show that in the warmest climate states, increasing oxygen may lead to a temperature decrease, as the equilibrium climate sensitivity is lower. For the Maastrichtian (72.1-–66.0 Ma), increasing oxygen content leads to a better agreement with proxy reconstructions of surface temperature at that time irrespective of the carbon dioxide content. For the Asselian (298.9–295.0 Ma), increasing oxygen content leads to a warmer global mean surface temperature and reduced carbon storage on land, suggesting that high oxygen content may have been a contributing factor in preventing a Snowball Earth during this period of the early Permian. These climate model simulations reconcile the surface temperature response to oxygen content changes across the hierarchy of model complexity and highlight the broad range of Earth system feedbacks that need to be accounted for when considering the climate response to changes in atmospheric oxygen content.

Clim. Past Discuss., https://doi.org/10.5194/cp-2018-149
Manuscript under review for journal Clim. Past
Discussion started: 14 December 2018

Climate of the Past Discussions
Open Access
EGU

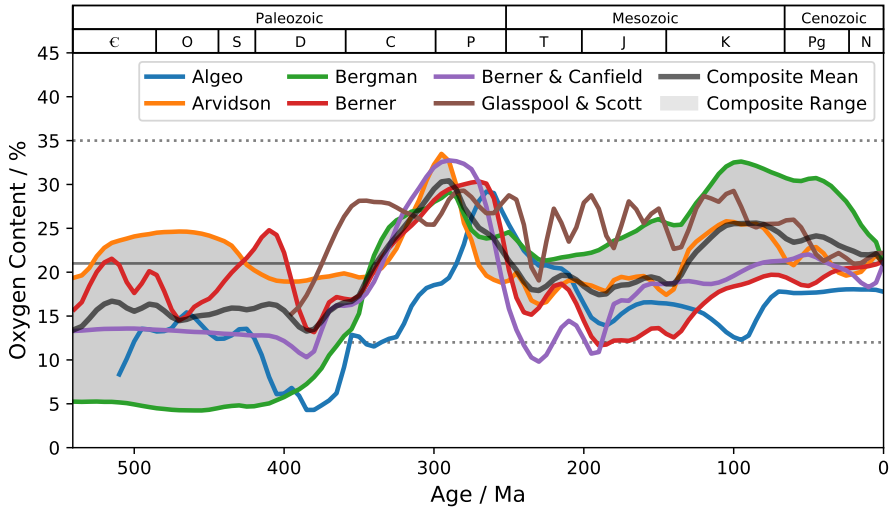

Figure 1. Oxygen content reconstructions in the Phanerozoic from Algeo and Ingall (2007), Arvidson et al. (2013), Bergman et al. (2004), Berner (2009), Berner and Canfield (1989) and Glasspool and Scott (2010). The mean (black line) and range (grey shading) of the Arvidson et al. (2013), Bergman et al. (2004) and Berner (2009) is indicated as these reconstructions were most consistent with ice core evidence (Stolper et al., 2016). High and low limits on atmospheric oxygen are indicated by horizontal grey dashed lines. Present day atmospheric oxygen content is indicated by the horizontal grey solid line.

1 Introduction

The primary driver of climate over the Phanerozoic is atmospheric CO_2 (Royer et al., 2004). However, atmospheric oxygen content may also have varied across the Phanerozoic. Atmospheric dioxygen (O_2) plays a vital role in the Earth system (Catling et al., 2005), regulating the biosphere through fire ignition (Watson et al., 1978) and metabolism of aerobic biota. Hence variability in the partial pressure of dioxygen (pO_2, a measure of the mass of O_2 in the atmosphere, assuming N_2 and the volume of the atmosphere have been constant) over time has been invoked as an evolutionary trigger (Berner et al., 2007) of both animals (Falkowski et al., 2005) and plants (He et al., 2012) at many points in the Phanerozoic (Saltzman et al., 2011; Robinson, 1990; Beerling and Berner, 2000; Scott and Glasspool, 2006; Edwards et al., 2017).

While strong biological and geological feedbacks prevent rapid swings in atmospheric oxygen (Catling and Claire, 2005), reconstructions of past atmospheric oxygen content suggest that there have been substantial excursions from the 21 % oxygen content present in today's atmosphere at times in the Phanerozoic eon. These reconstruction methods can be divided into forward and inversion models. Forward models include nutrient / weathering models (Bergman et al., 2004; Arvidson et al., 2013; Hansen and Wallmann, 2003) and isotope mass balance models (Berner 2009 and Falkowski et al. 2005) while inversion models infer oxygen content from proxies such as charcoal (Glasspool and Scott, 2010), organic carbon to phosphorus ratios (Algeo and Ingall, 2007) and plant resin $\delta^{13}C$ (Tappert et al., 2013). Figure 1 shows the reconstructed oxygen contents for a variety of these methods. There is general agreement in the trends in the reconstructions, in that that oxygen content increased

Clim. Past Discuss., https://doi.org/10.5194/cp-2018-149
Manuscript under review for journal Clim. Past
Discussion started: 14 December 2018

Climate of the Past Discussions

from 5-25% in the early Paleozoic to 20-35 % in the Permian. However, there is uncertainty in the absolute amount of O_2 for the different reconstructions (grey shading figure 1). Indeed, there is support for elevated O_2 by carbon isotope measurements (Beerling et al., 2002). However, disagreement is particularly evident in the Mesozoic, with low values simulated by isotope mass balance approaches. Mills et al. (2016) have shown that this could be due to an inappropriate choice of $\delta^{13}C$ and that adjusting this value with geological constraints leads to a higher reconstructed oxygen content in better agreement with wildfire records. At the time of writing, there are no direct geochemical proxies for pO_2 on the Phanerozoic timescale. However, pO_2 in the last 800 000 years has been reconstructed using O_2/N_2 ratios in ice cores (Stolper et al., 2016). A roughly 7‰ decline in pO_2 is consistent with the ability to change oxygen content by the order of a few percent in ~ 10 Myr. The reconstructions of Bergman et al. (2004), Arvidson et al. (2013) and Berner (2009) are the most plausible based on ice core data (Stolper et al., 2016). Considering these three models alone would still suggest a large uncertainty in oxygen content for most of the Phanerozoic, except for elevated levels in the late Carboniferous / early Permian and reduced levels in the late Devonian.

Phanerozoic means 'visible life' and the most marked change to carbon cycling between the Proterozoic and Phanerozoic was caused by the emergence of land plants. The radiation of land plants has led to strong regulation of atmosphere CO_2 and O_2 which both play important roles in photosynthesis. Land plants likely led to a substantial sequestration of carbon in the terrestrial biosphere and led to the Ordovician glaciation (Lenton et al., 2012). Increases in organic carbon sequestration in the aftermath of the evolution of lignin production may also have contributed to the cooling (Robinson, 1989). This fundamental change to the Earth system may have constrained CO_2 levels to between 10–200 Pa ever since (Franks et al., 2014) which is consistent with a long-term sensitivity of the Earth system to CO_2 changes (Royer, 2016). Watson et al. (1978) have argued that strong fire feedbacks prevent large fluctuations in oxygen levels, due to runaway burning at high oxygen levels. However subsequent experiments using natural fuels support the possibility of the Earth system to support higher oxygen levels (Wildman et al., 2004). Charcoal appears in the fossil record continuously since the late Silurian (~420 Ma, Scott and Glasspool 2006). This suggests a floor on oxygen levels in the region of 12% (Wildman et al., 2004) to 16% (Belcher and McElwain, 2008; Belcher et al., 2010) since then due to limits on ignition.

Variations in pO_2 also have important implications for photosynthesis and therefore the operation of the terrestrial carbon cycle. The primary CO_2-fixing enzyme, Rubisco, possesses a dual carboxylase-oxygenase function (Smith, 1976). A photosynthetic carboxylase pathway removes CO_2 from the atmosphere while oxygenation leads to photorespiration and CO_2 evolution. Therefore, increases in pO_2 ought to lead to O_2 outcompeting CO_2 for active sites on the Rubisco enzyme and leading to a reduction in net primary productivity (less photosynthesis, more respiration). However, photorespiration is likely to be necessary for removal of harmful byproducts in the photosynthetic metabolic pathway (Hagemann et al., 2016) and a recent study suggests that increases in photorespiration may actually promote photosynthesis (Timm et al., 2015). Photosynthesis is itself sensitive to the background CO_2 content (Beerling and Berner, 2000). In addition, temperature modifies the relative solubilities of CO_2 and O_2 (Jordan and Ogren, 1984). Temperature also affects the specificity of Rubisco for CO_2 (Long, 1991). Therefore, the coevolution of pO_2, pCO_2 and temperature across the Phanerozoic has the capacity to significantly impact the terrestrial carbon cycle.

Clim. Past Discuss., https://doi.org/10.5194/cp-2018-149
Manuscript under review for journal Clim. Past
Discussion started: 14 December 2018

Climate of the Past Discussions
Open Access
EGU

This paper focuses on investigating the climate impacts of atmospheric mass variation as the result of altering the concentration of O_2. Lower atmospheric mass leads to less Rayleigh scattering so more shortwave radiation reaches the Earth's surface. This enhances atmospheric convection and the hydrological cycle which leads to more tropospheric water vapour, further enhancing warming. However, lower atmospheric mass leads to a reduction in the pressure broadening of greenhouse gas absorption lines which should lead to a weaker greenhouse effect and lead to cooling. Previous modelling studies have investigated which factor dominates with conflicting results. Goldblatt et al. (2009) presented radiative-convective model simulations for the Archean (~3 Ga) which suggested that a nitrogen inventory around three times larger than present would help to keep the early Earth warm at a time when solar input was only around 75% of what it is today, potentially solving the 'Faint Young Sun' paradox (Feulner, 2012). Charnay et al. (2013) investigated this using a GCM coupled to a slab ocean and found that for their idealised early Earth simulations they achieved a strong warming (+7 °C) in response to a doubling in atmospheric mass. Poulsen et al. (2015) simulated the climate impacts of changes in O_2 content over a range of 5–35 % using the GENESIS climate model with a slab ocean and a continental configuration consistent with the Cenomanian (mid Cretaceous, 65 Ma) and found the opposite response – lower atmospheric mass at low pO_2 was associated with a strong warming. Subsequent 1D calculations cast doubt on this result (Goldblatt, 2016; Payne et al., 2016), however it is plausible that other climate feedbacks such as changes to relative humidity and cloud changes may be important as atmospheric mass changes. These would not be accounted for in 1D radiative-convective equilibrium simulations. Cloud feedbacks in particular are a good candidate for explaining the discrepancy as cloud feedbacks under CO_2-driven climate change have strong model dependency (Bony et al., 2015). Another feedback which has not been considered is the possible impact of changes in the mechanical forcing of wind on the ocean circulation. In the absence of this effect, Earth's surface temperature would be 8.7 K cooler (Saenko, 2009) and the equator-to-pole temperature gradient would be steeper. Wind stress (τ) is parameterized in GCMs as $\tau = \rho\, \mathbf{u} \cdot \mathbf{u}$ where ρ is the atmospheric density and $\mathbf{u}$ is the surface wind vector. So as atmospheric density increases, the wind stress on the ocean and therefore ocean heat transport should increase accordingly. Increased meridional heat transport in high density atmospheres is also supported by an idealised 2D modelling study of the early Earth (Chemke et al., 2016). As slab ocean models assume a constant or diffusive ocean heat transport, the Charnay et al. (2013) and Poulsen et al. (2015) simulations cannot account for these effects.

As pO_2 variability may alter the radiative budget of the atmosphere, it may also have impacts on the sensitivity of the climate state to CO_2 changes. The equilibrium climate sensitivity (ECS) is a metric for the sensitivity of a climate model to an abrupt doubling of atmospheric CO_2. Understanding this value is important for predictions of both past and future climatic changes. As the radiative forcing of CO_2 is approximately logarithmic with concentration, theoretically the ECS should be constant in time as carbon dioxide changes. However, there is growing evidence that ECS has not been constant over Earth's history (Caballero and Huber, 2013). Changes to the incoming solar radiation, palaeogeography (Lunt et al., 2016), CO_2 levels themselves (Meraner et al., 2013) and tropical sea-surface temperatures (Caballero and Huber, 2013) may lead to changes in the sensitivity of a particular climate state to changes in CO_2.

Clim. Past Discuss., https://doi.org/10.5194/cp-2018-149
Manuscript under review for journal Clim. Past
Discussion started: 14 December 2018

Climate of the Past Discussions
Open Access
EGU

2 Methods & Simulations

The impact of oxygen content variability is investigated with two coupled atmosphere-ocean general circulation models (AOGCMs): HadCM3BL and HadGEM3-AO.

HadGEM3-AO is an AOGCM (Nowack et al., 2014). The atmosphere component is the UK Met Office Unified Model version 7.3 (Davies et al., 2005) in the HadGEM3-A r2.0 climate configuration (Hewitt et al., 2011). It employs a regular Cartesian grid of 3.75° longitude by 2.5° latitude (N48). In the vertical, 60 hybrid height vertical levels are employed – 'hybrid' indicating that the model levels are sigma levels near the surface, changing smoothly to pressure levels near the top of the atmosphere (Simmons and Strüfing, 1983). The model top is 84 km which permits a detailed treatment of stratospheric dynamics. A 20 minute timestep is used. The model employs a non-hydrostatic and fully compressible dynamical core, using a semi-implicit semi-Lagrangian advection scheme on a staggered Arakawa C-grid (Awakawa and Lamb, 1977). Radiation is represented using the Edwards and Slingo (1996) scheme with six short-wave and nine long-wave bands, accounting for the radiative effects of water vapour, carbon dioxide, methane, nitrous oxide and ozone. The MOSES2 land surface scheme is used (Cox et al., 1999) which simulated atmosphere-land exchanges and hydrology. A fixed vegetation distribution of plant functional types is employed. The ocean component of the model is OPA component of the NEMO (Nucleus for European Modelling of the Ocean, Madec 2008) model version 3.0 (Hewitt et al., 2011), run at a 96 minute timestep. In the vertical, 31 model levels are used which increase steadily between 10 m in the shallowest to 500 m in the deepest layer at 5 km in depth. NEMO employs a tripolar, locally anisotropic grid (ORCA2, Madec 2008) which permits a more detailed treatment of the north polar region and higher resolution in the tropics. This yields an approximate horizontal resolution of 2° in both longitude and latitude, with an increased resolution of up to 0.5° in the tropics. The sea ice component of the model is CICE (Los Alamos Community Ice CodE) at version 4.0 (Hunke and Lipscomb, 2008), run at a 96 minute timestep. This treats sea-ice in a 5-layer model, allowing the simulation of different ice types. The atmosphere and ocean/sea-ice components exchange fields every 24 hours while NEMO and CICE exchange fields every timestep. HadGEM3-AO can be thought of as a close relation to the newest generation HadGEM3 coupled model that will be used to support the next IPCC assessment (Williams et al., 2018) and so represents the state-of-science in numerical climate models.

HadCM3BL (Valdes et al., 2017) is an AOGCM coupled to an interactive vegetation model. The model was originally developed by the United Kingdom Met Office Hadley Centre (Pope et al., 2000) but has since been substantially developed further by the University of Bristol. The atmosphere component of the model employs a regular Cartesian grid of 3.75° longitude by 2.5° latitude. In the vertical, 19 hybrid height vertical levels are employed. A 30 minute timestep is used. The primitive equation set of White and Bromley (1995) is solved to conserve energy and angular momentum, solved on a staggered Awakawa B-grid (Awakawa and Lamb, 1977) in the horizontal. Radiation is represented using the Edwards and Slingo (1996) scheme with six short-wave and eight long-wave bands, accounting for the radiative effects of water vapour, carbon dioxide and ozone, amongst other radiative active species. The ocean component of the model employs the same horizontal grid as the atmosphere component of the model, 3.75° longitude by 2.5° latitude. In the vertical, 20 model levels are used which increase in depth from 10 m in the shallowest layer to 616 m in the deepest layer. A timestep of 60 minutes is employed and the ocean and atmosphere

Clim. Past Discuss., https://doi.org/10.5194/cp-2018-149
Manuscript under review for journal Clim. Past
Discussion started: 14 December 2018

Climate of the Past Discussions
Open Access
EGU

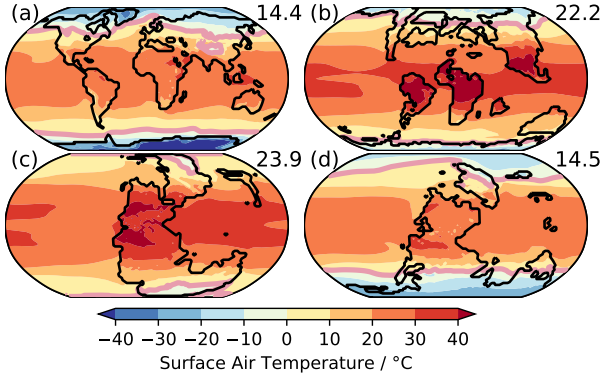

Figure 2. Annual average surface air temperature simulated in (a) PI-CM[21], (b) Ma-CM[21], (c) Wu-CM[21] and (d) As-CM[21]. Global mean values are inset top right. The 0 Celsius isoline is indicated in pink.

components exchange required fields once per day. The ocean component is based on the Cox (1984) model, solving the full primitive equation set in three-dimensions. A staggered Awakawa B-grid is employed in both atmosphere and ocean models. Sea-ice is treated as a zero thickness layer on the surface of the ocean grid. Ice is assumed to form at the base at a freezing point of –1.8 °C but can also form from freezing in ice leads and by falling snow. A simple parameterisation of sea-ice dynamics is also employed (Gordon et al., 2000) and sea-ice formation due to convergence from drift is limited to 4 m deep. Sea-ice albedo is fixed at 0.8 for temperatures below –10 °C, decreasing linearly to 0.5 at 0 °C. The MOSES2.1 land surface model is employed to simulate the fluxes of energy and water between the land surface and the atmosphere (Cox et al., 2000; Essery et al., 2003). TRIFFID (Top-down Representation of Interactive Foliage and Flora Including Dynamics, Cox et al. 1998) predicts the distribution of vegetation using a plant functional type (PFT) approach. TRIFFID is run in equilibrium mode with averaged fluxes calculated over a 5 year period. TRIFFID calculates vegetation properties for five PFTs: broadleaf trees, needleleaf tree, C3 grass, C4 grass and shrubs. Gridboxes can contain a mixture of PFTs based on a 'fractional coverage co-existence approach' Valdes et al. (2017). Net primary productivity (NPP) is also calculated, using a photosynthesis-stomatal conductance model (Cox et al., 1998) accounting for a number of factors including atmospheric oxygen content. The predicted vegetation distribution impacts the atmosphere component by altering surface albedo, evapotranspiration and surface roughness. Simulations have been run for 1422 model years reaching an equilibration state at the surface.

Both models simulated the climate response to oxygen variability in a preindustrial Holocene (PIH) climate. HadCM3-BL was additionally run for three time periods across the Phanerozoic: The Maastrichtian (late Cretaceous, 66.0–72.1 Ma), Wuchiapingian (late Permian, 254.14–259.1 Ma) and the Asselian (early Permian, 295.0–298.9 Ma) as it is possible to alter the model topography and bathymetry. The continental reconstructions employed were developed by and are ©Getech. These reconstructions have been widely employed in a number of previous studies using the HadCM3-BL climate model (e.g. (Lunt et al., 2016)). All three are periods of time in which models have suggested that atmospheric oxygen may have deviated significantly from the present level of 21 % (see Fig. 1). Modifications were made to alter the oxygen content of the atmosphere

Clim. Past Discuss., https://doi.org/10.5194/cp-2018-149
Manuscript under review for journal Clim. Past
Discussion started: 14 December 2018

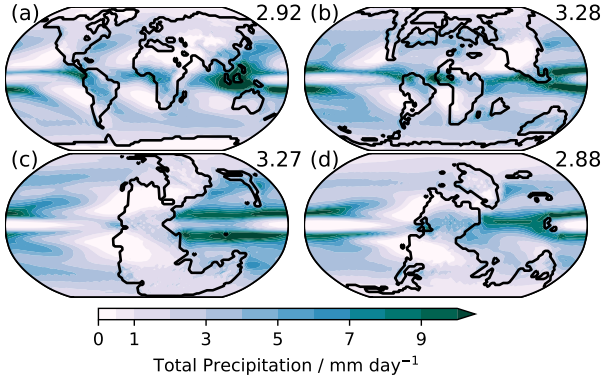

Figure 3. Annual average precipitation simulated in (a) PI-CM^{21}, (b) Ma-CM^{21}, (c) Wu-CM^{21} and (d) As-CM^{21}. Global mean values are inset top right.

Table 1. Summary of experiments.

Experiment	Continents	Model	CO_2 / Pa	O_2 / %	Notes
PI-GEM	PIH	HadGEM3-AO	28	10,21,35	
4xPI-GEM	PIH	HadGEM3-AO	112	10,35	
PI-CM	PIH	HadCM3-BL	28	10,21,35	
Ma-CM	Maastrichtian	HadCM3-BL	56	10,21,35	
As-CM	Asselian	HadCM3-BL	28	10,21,35	
Wu-CM	Wuchiapingian	HadCM3-BL	112	10,21,35	
τPI-CM*	PIH	HadCM3-BL	28	21	1
τMa-CM*	Maastrichtian	HadCM3-BL	56	21	1
τAs-CM*	Asselian	HadCM3-BL	28	21	1
τWu-CM*	Wuchiapingian	HadCM3-BL	112	21	1
PI2x-CM*	PIH	HadCM3-BL	56	10,21,35	
Ma2x-CM*	Maastrichtian	HadCM3-BL	112	10,21,35	
As2x-CM*	Asselian	HadCM3-BL	56	10,21,35	

Notes: 1) Wind stress to ocean set to zero.

by adjusting the mass mixing ratios of major and minor gases, the surface pressure and other physical characteristics of the atmosphere such as the specific gas constant in an analogous way to Poulsen et al. (2015). The annual average surface temperatures and annual average precipitation for PI-CM^{21}, PI-CM^{21}, PI-CM^{21} and PI-CM^{21} simulations are shown in Figs. 2 and 3.

Clim. Past Discuss., https://doi.org/10.5194/cp-2018-149
Manuscript under review for journal Clim. Past
Discussion started: 14 December 2018

Climate of the Past Discussions

A summary of the experiments performed can be found in Table 1. When an experiment with a particular oxygen content is referred to, it will be indicated in superscript, e.g. EXP^{21} indicates a 21 % oxygen simulation. 21 % simulations (PI-CM^{21}, As-CM^{21}, Ma-CM^{21} and Wu-CM^{21}) were integrated for 50 model years as these simulations had already been spun up at that CO_2 content. For 10 % and 35 % O_2 the model was spun off the 21 % O_2 simulation and iterated for at least 1000 model years. The PI2x-CM*, Ma2x-CM* and As2x-CM* experiments were spun off from the end of the PI-CM, Ma-CM and As-CM experiments and iterated for 100, 1000 and 100 years respectively. For HadGEM3-AO, model integrations (PI-GEM^{35}, PI-GEM^{10}, 4xPI-GEM^{35} and 4xPI-GEM^{10}) were performed for 300 model years with a 10-times acceleration of the deep ocean to reduce the time for equilibrium then integrated for a further 500 years to spin up the shallow ocean without acceleration. The last 50 years were used for model analysis.

Pre-Quaternary pCO_2 is poorly constrained due to the absence of glacial ice, however there is growing evidence that CO_2 is unlikely to have been significantly higher than ~100 Pa since the radiation of land plants (Breecker et al., 2010; Franks et al., 2014). For the Maastrichtian, 56 Pa is used in agreement with stomatal proxy-based reconstructions (Steinthorsdottir and Pole, 2016). For the Asselian, 28 Pa is used in agreement with carbonate and fossil plant reconstructions (Montañez et al., 2007). For the Wuchiapingian, 112 Pa is used (Brand et al., 2012).

1D atmospheric chemistry simulations have simulated higher O_3 column with increasing pO_2 (Kasting et al., 1979; Payne et al., 2016). More detailed 2D model simulations, which capture critical latitudinal gradients in photolysis and zonal mean transport (Hadjinicolaou and Pyle, 2004; Haigh and Pyle, 1982), support a monotonically increasing ozone column with increasing pO_2 (Harfoot et al., 2007). However, simulated ozone column was more sensitive to N_2O levels than pO_2 (Harfoot et al., 2007). In addition, while column ozone reduces at low pO_2 in Harfoot et al. (2007) there are increases in ozone concentration in the tropical tropopause region where the radiative effect of O_3 is stronger (Forster and Shine, 1997). Changes in lightning are important for understanding future changes in tropospheric ozone (Banerjee et al., 2014), however are subject to considerable uncertainty (Finney et al., 2018). There may be more lightning at high pO_2 due to a higher pO_2/pN_2 ratio or less due to reduced convection (Goldblatt et al., 2009). Low pO_2 may also enhance isoprene emissions (Rasulov et al., 2009), which could enhance tropospheric ozone and alter cloud properties (Kiehl and Shields, 2013). Ozone is also sensitive to changes in CH_4 and N_2O, the changes to inventories of these chemically-active species on the Phanerozoic timescale (Beerling et al., 2009, 2011) is highly uncertain. Ozone is also sensitive to dynamical changes. Given these large uncertainties in possible changes to chemical sources, reactivity and transport we neglected including changes in atmospheric ozone concentration in these simulations. However, we recommend that follow up work should focus on this specific question in detail. In HadGEM3-AO the mass of tropospheric and stratospheric ozone is fixed at PIH values simulated by (Nowack et al., 2014) using a tropopause height matching scheme. This prevents a rising tropopause leading to stratospheric levels of ozone existing in the troposphere, particularly in the 4xPI-GEM experiments. Not accounting for a rising tropopause has been found to artificially increase climate sensitivity (Heinemann, 2009) and initial tests not accounting for this led to instability for 4xPI-GEM^{10}. In HadCM3-BL, tropospheric ozone is set to 6 ppbv and stratospheric ozone is set to 1.66 ppmv for the 21 % simulations. These values are adjusted to conserve total ozone mass in the alternative pO_2 scenarios.

Clim. Past Discuss., https://doi.org/10.5194/cp-2018-149
Manuscript under review for journal Clim. Past
Discussion started: 14 December 2018

Climate of the Past Discussions

Proxy data for the Maastrichtian was obtained from Upchurch et al. (2015) and interpolated from their modern locations on to the ©Getech grid. Where the proxy locations deviated substantially from those described in Upchurch et al. (2015) (i.e. terrestrial proxy in the ocean) these were adjusted heuristically. The proxy data was obtained by a variety of methods including TEX_{86}, $\delta^{18}O$ and leaf margin analysis. A full description of the proxy data and methods used can be found in Upchurch et al. (2015) and reference therein. Data for the Cenomanian Poulsen et al. (2015) 21 % O_2 and 10 % O_2 simulations were obtained from https://www.ncdc.noaa.gov/paleo/study/18776. At the time of writing the 35 % simulation contained missing data so was not used for analysis.

A 1D energy balance model (EBM) has been used to deconvolve the contributions from changes in different parts of the climate system. This 1D-EBM approach has been applied to zonal mean quantities for climate simulations of the Eocene by Heinemann et al. (2009) following Budyko (1969) and Sellers (1969):

$$\mathrm{SW}_t^{\downarrow}(\phi)[1-\alpha(\phi)] - \frac{1}{2\pi R^2 \cos(\phi)} \frac{\partial F(\phi)}{\partial \phi} = \epsilon(\phi)\sigma T_{s,\mathrm{ebm}}^4(\phi) \tag{1}$$

where $\mathrm{SW}_t^{\downarrow}$ is the incident shortwave radiation at the top-of-the atmosphere, ϕ is the latitude, α is the surface albedo, R is the radius of Earth, ϵ is the effective surface emissivity and $T_{s,\mathrm{ebm}}$ is the EBM surface temperature (Heinemann et al., 2009). $\frac{\partial F(\phi)}{\partial \phi}$ is the divergence of total meridional heat transport and is given by

$$\frac{\partial F(\phi)}{\partial \phi} = -2\pi R^2 \cos(\phi)(\mathrm{SW}_t^{\mathrm{net}}(\phi) + \mathrm{LW}_t^{\mathrm{net}}(\phi)) \tag{2}$$

where $\mathrm{SW}_t^{\mathrm{net}}$ and $\mathrm{LW}_t^{\mathrm{net}}$ are the net top-of-atmosphere shortwave and longwave radiative fluxes respectively (positive downward, Heinemann et al. 2009). Solving for $T_{s,\mathrm{ebm}}$, the EBM surface temperature for each latitude can be calculated using zonal and annual mean radiative fluxes from the GCM. Where clear-sky radiative fluxes are also available, cloud radiative effects can be deconvolved from clear-sky radiative effects. The clear-sky albedo α_c and clear-sky effective surface emissivity ϵ_c can be calculated by:

$$\alpha_c = \frac{\mathrm{SW}_{t,c}^{\uparrow}}{\mathrm{SW}_t^{\downarrow}}, \epsilon_c = \frac{\mathrm{LW}_{t,c}^{\uparrow}}{\mathrm{LW}_s^{\uparrow}} \tag{3}$$

where $SW_{t,c}^{\uparrow}$ is the upward top-of-atmosphere clear-sky shortwave radiative flux and $LW_{t,c}^{\uparrow}$ is the upward top-of-atmosphere clear-sky longwave radiative flux. When considering the temperature change between two experiments, the contributions from different components can be quantified by calculating $\tau_{s,\mathrm{ebm}}$ with different combinations of components from each experiment (Heinemann et al., 2009).

To estimate the climate sensitivity to CO_2 changes, the linear regression methodology of Gregory et al. (2004) is employed. This assumes a linear relationship between the changes in global, annual mean radiative imbalance at the top-of-atmosphere (N, Wm^{-2}) and surface temperature anomalies (T_s, °C)

$$N = F + \xi \Delta T_\mathrm{s} \tag{4}$$

where ξ is the effective climate feedback parameter ($\mathrm{Wm}^{-2}\,^{\circ}\mathrm{C}^{-1}$) and F is the effective forcing (Wm^{-2}) accounting for fast climate adjustments and effective radiative forcing. The effective ECS is then ΔT_s when $N = 0$. While there are weaknesses

Clim. Past Discuss., https://doi.org/10.5194/cp-2018-149
Manuscript under review for journal Clim. Past
Discussion started: 14 December 2018

of this approach, particularly due to non-linearities in ξ as ΔT_s changes (Armour et al., 2013; Li et al., 2013), the climate response when simulations are continued to equilibrium show an accuracy to within 10 % (Li and Sharma, 2013). Furthermore, the contributions to ξ and F from longwave (LW) and shortwave (SW), clear-sky (CS) and cloudy-sky (CRE) components can be decomposed by a linear decomposition as

$$F = F_{\mathrm{CS,SW}} + F_{\mathrm{CS,LW}} + F_{\mathrm{CRE,SW}} + F_{\mathrm{CRE,LW}} \tag{5}$$

for the effective forcing and

$$\xi = \xi_{\mathrm{CS,SW}} + \xi_{\mathrm{CS,LW}} + \xi_{\mathrm{CRE,SW}} + \xi_{\mathrm{CRE,LW}} \tag{6}$$

for the effective climate feedback parameter.

3 Results

Where results are presented from a single simulation, the oxygen content for that run is superscript, i.e. EXP^{21} indicates a 21 % oxygen simulation. Where results are presented as an anomaly between simulations with different oxygen contents, EXP_0^{21} indicates that the quantity presented is EXP^{21} minus EXP^{0}. A summary of results is shown in Table 2.

3.1 Surface Climate

Figure 4 (left) shows the annual-mean surface air temperature differences between the 35 % and 10 % runs. For the preindustrial Holocene, PI-GEM_{10}^{35} shows a global mean surface temperature response of +1.50 °C while PI-CM_{10}^{35} shows a similar global mean surface temperature response of +1.22 °C, also suggesting this is not a model dependent result. This is in reasonable agreement with the 1-D results of Payne et al. (2016) who simulated a temperature response between +1.05 and +2.21 °C depending on assumptions about atmospheric ozone. Similarly, the As-CM_{10}^{35} case exhibits a global mean surface temperature response of +1.29 °C. For the warmest climates, a response of –0.82°C is simulated for WU-CM_{10}^{35} and +0.17 °C for 4xPI-GEM_{10}^{35}. In the Ma-CM_{10}^{35} case, a global mean surface temperature response of +0.70 °C is simulated. This suggests that oxygen content can modulate the climate response to $\mathrm{CO_2}$ changes, but is non-linear due to various competing Earth system feedbacks.

There is a strong seasonal dependence in the surface air temperature response. Considering the changes in coolest average monthly temperature in each gridbox (Figure 4 centre), the change in cool month dominates the warming response, particularly at high latitudes. By contrast, the warm month mean is smaller/less negative in all cases (Figure 4 right). A cooling of continental land masses is evident in the tropics and particularly in the Wu-CM and 4xPI-GEM cases. These could be in part due to free-air lapse rate changes which should be stronger at high $p\mathrm{O_2}$ as for a given topographic height, the change in pressure is higher for high $p\mathrm{O_2}$ which should lead to a larger temperature reduction with height. The changes to the seasonal cycle are consistent with the radiative changes associated with changing oxygen content. The reduction in incident surface shortwave radiation should have its strongest effect on extratropical temperatures in the summer, therefore the Rayleigh scattering component will most strongly affect the warm month temperature. Warming from pressure broadening of greenhouse gas absorption

Clim. Past Discuss., https://doi.org/10.5194/cp-2018-149
Manuscript under review for journal Clim. Past
Discussion started: 14 December 2018

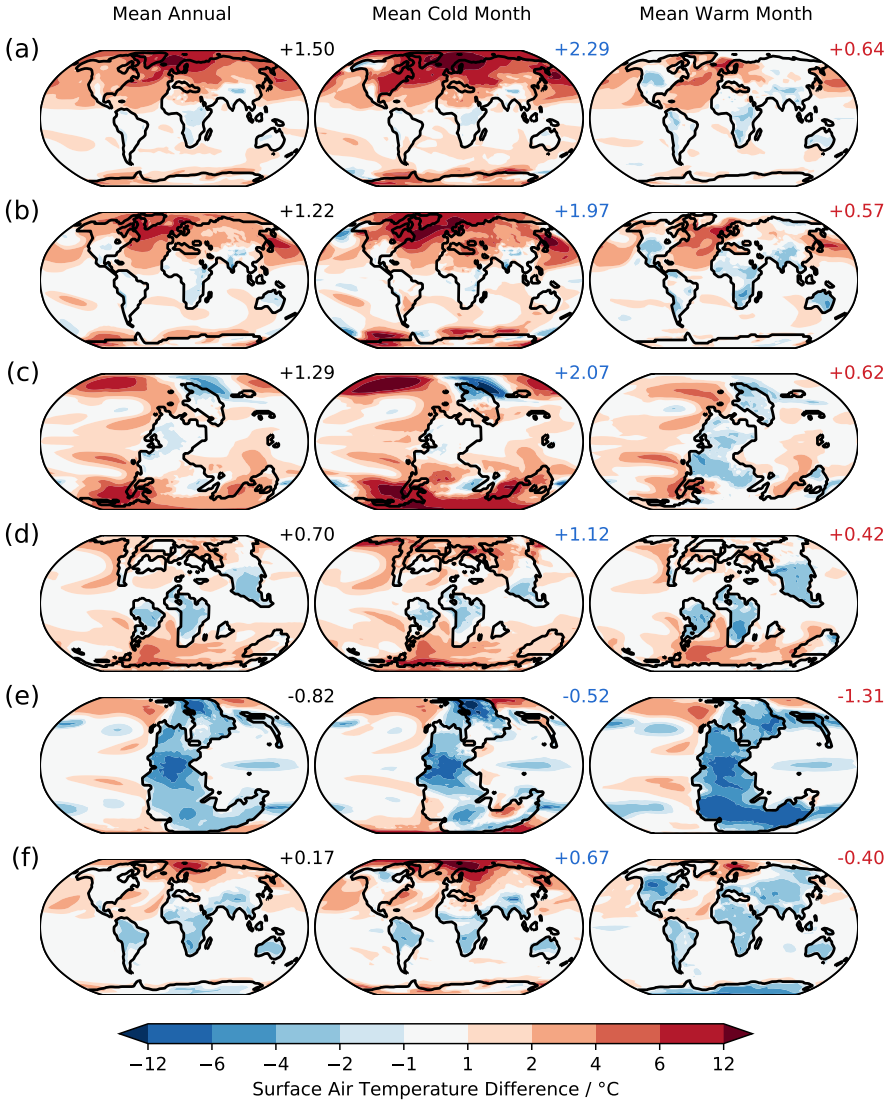

Figure 4. Surface air temperature change for (a) PI-GEM$^{35}_{10}$, (b) PI-CM$^{35}_{10}$, (c) As-CM$^{35}_{10}$, (d) Ma-CM$^{35}_{10}$, (e) Wu-CM$^{35}_{10}$ and (f) 4xPI-GEM$^{35}_{10}$ in the annual mean (left), cold month mean (centre) and warm month mean (right). The change in global mean values (°C) are offset to the top-right of each plot. Note the strong high latitude warming in the cold month mean and tropical cooling in the warm month mean.

Clim. Past Discuss., https://doi.org/10.5194/cp-2018-149
Manuscript under review for journal Clim. Past
Discussion started: 14 December 2018

Climate of the Past Discussions

Table 2. Summary of results for EXP^{21} then EXP^{35}_{10}. Where applicable, results calculated for the Poulsen et al. (2015) Cenomanian 21 %–10 % oxygen simulation are also presented. Abbreviations: $T_{\text{eq-pole}}$ (Equator-to-pole surface air temperature gradient), $T_{\text{eq-pole,cold month}}$ (Equator-to-pole surface air temperature gradient for cold month), EBM (quantities obtained using a Budyko-Sellers 1D energy balance model following Heinemann 2009), $T_{\text{s,ebm}}$ (EBM Surface temperature), $T_{\text{s,csky,ebm}}$ (EBM Surface temperature change accounting for changes in clear sky radiative fluxes), $T_{\text{s,cre,ebm}}$ (EBM Surface temperature change accounting for changes in cloudy sky radiative fluxes), $T_{\text{s,mht,ebm}}$ (EBM Surface temperature change accounting for changes in meridional heat flux divergence)

Quantity	PI-GEM	4xPI-GEM	PI-CM	As-CM	Ma-CM	Wu-CM	Poulsen
pCO_2 / Pa	28	112	28	28	56	112	56
			EXP^{21}				EXP^{21}
T_s / °C	14.3	—	14.4	14.5	22.2	23.9	20.5
Precip. / mm day^{-1}	3.11	—	2.92	2.88	3.28	3.27	3.49
			EXP^{35}_{10}				EXP^{21}_{10}
GCM T_s /°C	+1.35	+0.05	+1.14	+1.19	+0.57	–1.01	–2.06
$T_{\text{eq-pole}}$ / °C	–4.15	–2.18	–3.11	–2.38	–2.28	–1.92	+0.93
$T_{\text{eq-pole,cold month}}$ / °C	–6.53	–4.17	–5.07	–5.61	–3.91	–2.50	+1.89
Planetary Albedo	+0.008	+0.015	+0.001	+0.002	–0.003	+0.006	+0.009
Surface Emissivity	–0.019	–0.011	–0.011	–0.013	–0.003	+0.004	+0.008
$T_{\text{s,ebm}}$ / °C	+1.30	+0.10	+1.10	+1.08	+0.53	–1.01	–2.05
$T_{\text{s,csky,ebm}}$ / °C	+1.51	+0.05	+1.45	+1.35	+0.90	–0.30	–0.60
$T_{\text{s,cre,ebm}}$ / °C	–0.43	–0.13	–0.57	–0.49	–0.36	–0.58	–1.25
$T_{\text{s,mht,ebm}}$ / °C	+0.22	+0.18	+0.22	+0.22	–0.01	–0.13	–0.20

lines as atmospheric mass increases will be most evident in extratropical winter, as with anthropogenic climate change, due to sea-ice and surface heat flux changes (Dwyer et al., 2012). The reduction in the amplitude of the seasonal cycle in temperature simulated by both HadGEM3-AO and HadCM3-BL is therefore supported by a consideration of the changes to atmospheric radiation.

The zonal and annual mean surface air temperature changes are shown in Fig. 5. The Northern Hemisphere equator-to-pole temperature gradient is reduced by 6.6 °C in the PI-GEM^{35}_{10} case (blue line) and 4.0 °C in the PI-CM^{35}_{10} case (not shown). The zonal structure of the surface temperature change is similar in the palaeoclimate case studies. In the Maastrichtian, the equator-to-pole temperature gradient is reduced by 2.0 °C (Ma-CM^{35}_{10}) and in the Asselian the equator-to-pole temperature gradient is reduced by 2.3 °C (As-CM^{35}_{10}). Comparing the surface temperature and precipitation response between HadCM3-BL and HadGEM3-AO suggests that the model responses are broadly consistent. The equator-to-pole temperature gradient reduces even in the Wu^{35}_{10} case despite the reduction in global mean surface temperatures. A gridbox-by-gridbox comparison of annual mean surface air temperature and precipitation anomalies for PI-GEM^{35}_{10} vs PI-CM^{35}_{10} is presented in Fig. S1. The largest discrepancy in surface air temperature response between the two models occurs for the largest temperature changes simulated by HadGEM, which is strongest in Northern Hemisphere polar regions. This could be linked to differences in the

Clim. Past Discuss., https://doi.org/10.5194/cp-2018-149
Manuscript under review for journal Clim. Past
Discussion started: 14 December 2018

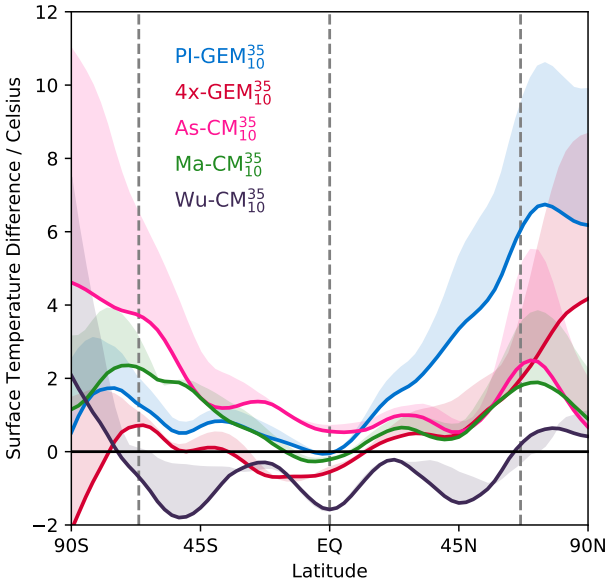

Figure 5. Zonally and annually averaged surface air temperature difference (solid lines) from 10 % to 35 % oxygen content for PI-GEM (blue), 4xPI-GEM(red), As-CM (pink), Ma-CM (green) and Wu-CM (purple). The difference from the annual-mean to cold month-mean for each run is indicated by the shading. Values are smoothed by a Savitzky-Golay filter (Savitzky and Golay, 1964).

representation of polar climate processes between the two models. There is broad consistency in cold and warm-month means (Figure 4a and b) with stronger warming in the cold month mean and terrestrial cooling in the warm month mean.

The hydrological cycle is also affected by changing oxygen content. Increases in Rayleigh scattering at high pO_2 ought to reduce incident shortwave at Earth's surface (Poulsen et al., 2015) and inhibit convection (Goldblatt et al., 2009) which should lead to reductions in precipitation. This is analogous to stratospheric sulfate or solar radiation management geoengineering where precipitation is reduced in geoengineering experiments with respect to an unperturbed climate with the same global mean surface temperature (Irvine et al., 2016). Poulsen et al. (2015) simulated large reductions in precipitation as pO_2 increased in the GENESIS climate model, however much of this could be explained by the surface temperature changes. Annually averaged precipitation change between the 10 % and 35 % oxygen content runs are show in Fig. 6. In all cases, increasing oxygen content leads to a decline in global mean total precipitation, despite the increase in surface temperatures, however with strong regional differences. For PI-GEM, PI-CM and 4xPI-GEM there is a clear northward shift in the tropical rain belts. A northward shift in the ITCZ would be consistent with stronger warming in the Northern Hemisphere. Heat transport is more hemispherically symmetric in the Maastrichtian, Asselian and Wuchiapingian cases so latitudinal ITCZ shifts are not evident. While global precipitation is reduced in Wu-CM^{35}, the increase in ocean-land temperature contrast leads to a significant increase in tropical land precipitation which suggests that pO_2 could mediate monsoon circulations. Despite the increases in global-mean surface temperatures simulated for most cases, precipitation is still reduced in all simulations.

Clim. Past Discuss., https://doi.org/10.5194/cp-2018-149
Manuscript under review for journal Clim. Past
Discussion started: 14 December 2018

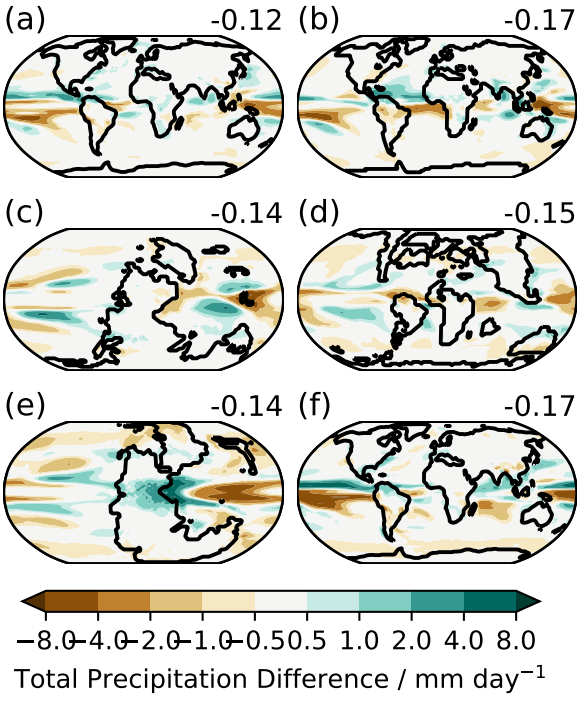

Figure 6. Annually averaged total precipitation change from 10 % to 35 % oxygen content for (a) PI-GEM$^{35}_{10}$, (b) PI-CM$^{35}_{10}$, (c) As-CM$^{35}_{10}$, (d) Ma-CM$^{35}_{10}$, (e) Wu-CM$^{35}_{10}$ and (f) 4xPI-GEM$^{35}_{10}$. Global mean values (mm day^{-1}) are offset.

3.2 Energy Balance Decomposition

The drivers of the changes in surface temperature can be understood by decomposing the terms which contribute to surface temperature change in a 1D-energy balance model following Heinemann et al. (2009). For PI-CM$^{35}_{10}$, these results are shown in Fig. 7. These show that the 1D-EBM can reasonably capture the temperature response in the HadCM3-BL simulations, with slight errors (where the black and grey lines are not overlapping) evident in the polar regions. This could be due to averaging over the polar rows in the HadCM3-BL model. There are positive contributions to the surface temperature change in the clear sky emissivity and albedo at the poles. This is consistent with the increase in pressure broadening of absorption lines and the simulated reduction in sea-ice extent. By contrast, extrapolar contributions to clear sky albedo provide a negative contribution to the temperature change which is consistent with an increase in Rayleigh scattering which would be expected to be strongest in the tropics where the maximum in incoming solar radiation is located. Combined, the clear sky component of the temperature change is +1.45°C and the cloudy sky component is –0.35°C. This suggests that HadCM3-BL supports a cloud feedback which acts to cool the climate at high pO_2 and partially offset the clear-sky temperature changes.

The same analysis was performed for the HadGEM3-AO PIH simulations. Fig. 8 shows that a somewhat weaker cloud feedback is simulated by HadGEM3-AO (–0.21°C). Clear-sky contributions are slightly stronger (+1.51°C). The largest dif-

Clim. Past Discuss., https://doi.org/10.5194/cp-2018-149
Manuscript under review for journal Clim. Past
Discussion started: 14 December 2018

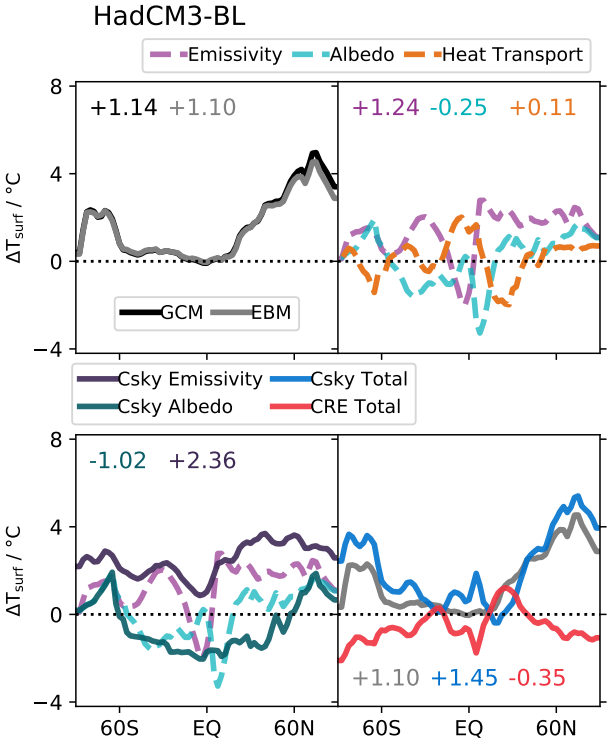

Figure 7. 1D-EBM decomposition for PI-CM$^{35}_{10}$. Top left: EBM results (grey) vs GCM results (black). Top right: Decomposition of EBM into the emissivity (purple), albedo (green) and heat transport (orange) components of the temperature change. Bottom left: Clear-sky emissivity (dark purple) and albedo (dark green) components of the EBM. Bottom right: Decomposition of EBM into the total clear-sky (blue), cloudy-sky (red) and all-sky (grey) components.

ferences between the simulations appear in the all-sky albedo and emissivity changes, where there appear to be competing factors which lead to a similar climate response possibly related to partitioning between the longwave and shortwave contributions to the cloud response. This is perhaps unsurprising, as cloud feedbacks to CO_2 changes represent a large uncertainty in future climate change projections and given the relatively small global-mean temperature changes a relatively small change in cloud radiative effects has the power to considerably mediate the climate response. However the qualitative agreement in latitudinal structure of the clear sky albedo and emissivity changes between these structurally different models gives some confidence that the relevant climate feedbacks are well captured in these simulations.

Analysis of the palaeo-case studies (As-CM, Fig. S2; Ma-CM, Fig. S3; Wu-CM, Fig. S4) shows a similar pattern. In all simulations, irrespective of surface temperature response, the clear sky emissivity is a positive contribution to global mean surface temperature change while clear sky albedo is a more negative contribution. The emissivity contribution becomes less positive as pCO_2 increases from As-CM to Ma-CM to Wu-CM. By contrast the albedo contribution becomes more negative

Clim. Past Discuss., https://doi.org/10.5194/cp-2018-149
Manuscript under review for journal Clim. Past
Discussion started: 14 December 2018

Climate of the Past Discussions
Open Access
EGU

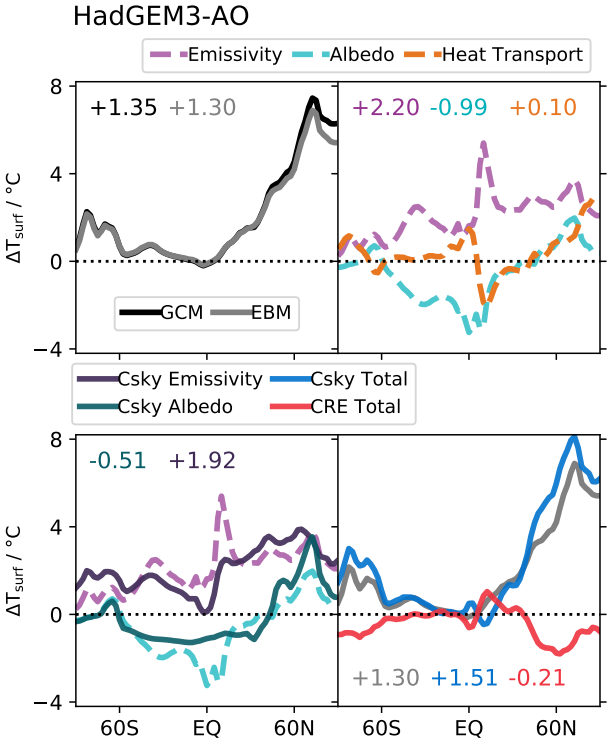

Figure 8. 1D-EBM decomposition for PI-GEM$^{35}_{10}$. Top left: EBM results (grey) vs GCM results (black). Top right: Decomposition of EBM into the emissivity (purple), albedo (green) and heat transport (orange) components of the temperature change. Bottom left: Clear-sky emissivity (dark purple) and albedo (dark green) components of the EBM. Bottom right: Decomposition of EBM into the total clear-sky (blue), cloudy-sky (red) and all-sky (grey) components.

as $p\mathrm{CO}_2$ increases. This is consistent with the reduction in planetary albedo as sea-ice extent is reduced on the ocean and dark vegetated surfaces increase on the land.

3.3 Climate Sensitivity

Here we investigate the impact of oxygen variability on climate sensitivity. The HadGEM3-AO and HadCM3-BL results suggest that increasing CO_2 content leads to a reduction in the surface temperature change on increasing $p\mathrm{O}_2$ (compare 4xPI-GEM and PI-GEM in Fig. 4). From the 4xPI-GEM and PI-GEM experiments, a reduction in climate sensitivity of 0.65°C can be inferred, based on the changes in surface temperatures. For HadCM3, CO_2-doubling experiments were performed and a regression of the change in top-of-atmosphere radiative imbalance against change in surface temperature following Gregory et al. 2004 (see also section 2) is shown in Fig. 9. The PI-CM^{35} climate state has a smaller ECS than PI-CM^{10} by 0.7°C. While the changes in total radiative forcing F are very similar, ξ is less negative (-1.08 vs -1.37 $\mathrm{Wm}^{-2}\,^{\circ}\mathrm{C}^{-1}$) at low $p\mathrm{O}_2$. The decomposition of these changes into their longwave and shortwave components, clear-sky and cloudy-sky components

Clim. Past Discuss., https://doi.org/10.5194/cp-2018-149
Manuscript under review for journal Clim. Past
Discussion started: 14 December 2018

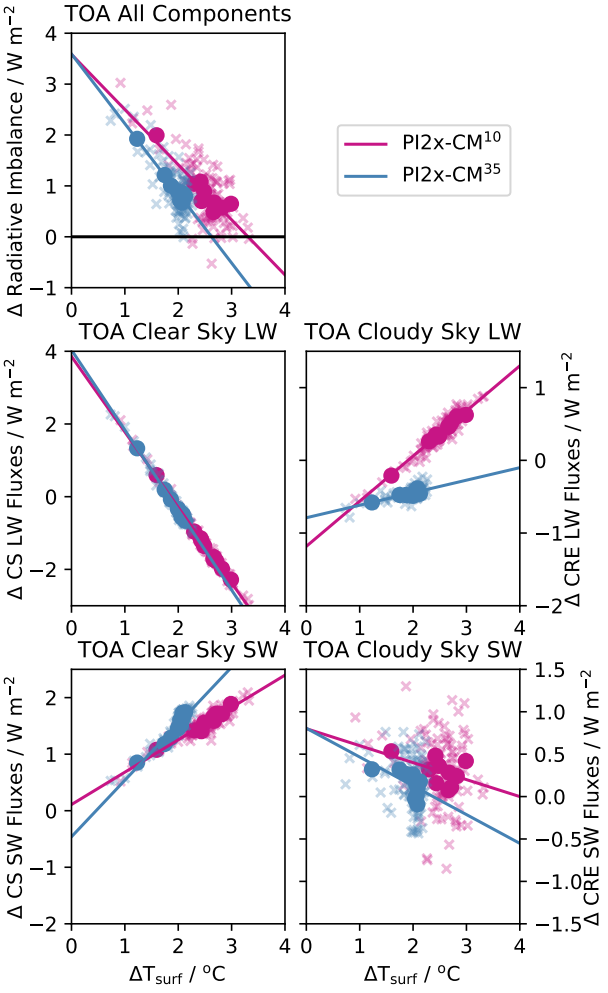

Figure 9. Gregory analysis of HadCM3-BL: Regression of top-of-atmosphere radiative balance against surface air temperature change (solid lines) for the first 100 years of PI2x-CM^{10} (pink) and PI2x-CM^{35} (blue) cases. Annual averages are indicated by crosses and decadal averages are indicated by filled circles. The regression was performed on the decadal averages.

Clim. Past Discuss., https://doi.org/10.5194/cp-2018-149
Manuscript under review for journal Clim. Past
Discussion started: 14 December 2018

Climate of the Past Discussions

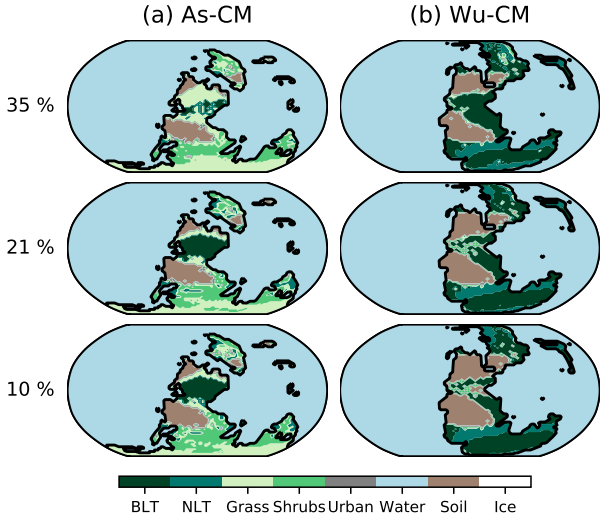

Figure 10. Dominant surface type for each oxygen level simulation for (a) As-CM and (b) Wu-CM. BLT: Broadleaf trees, NLT: Needleleaf trees.

is also shown in Fig. 9. The clear-sky longwave radiative flux changes are higher in PI2x-CM^{35} (4.0$\mathrm{Wm^{-2}}$) than PI2x-CM^{10} (3.8$\mathrm{Wm^{-2}}$) as would be expected due to the pressure broadening of $\mathrm{CO_2}$. The clear driver for the less negative ξ value are from the longwave cloud radiative effect changes which is much steeper for PI2x-CM^{10} (+0.62$\mathrm{Wm^{-2}\,{}^{\circ}C^{-1}}$) than PI2x-CM^{35} (+0.17$\mathrm{Wm^{-2}\,{}^{\circ}C^{-1}}$). This is somewhat offset by stronger clearsky shortwave radiative feedbacks in PI2x-CM^{35} (+1.00$\mathrm{Wm^{-2}\,{}^{\circ}C^{-1}}$) than PI2x-CM^{10} (+0.57$\mathrm{Wm^{-2}\,{}^{\circ}C^{-1}}$). This highlights the important role that cloud radiative feedbacks play in determining the climate sensitivity.

An increase in ECS appears to be robust across the HadCM3-BL experiments. For As-CM, ECS is 0.8°C lower at 35 % $\mathrm{O_2}$ than 10 % $\mathrm{O_2}$ (see also Fig. S5). For Ma-CM, this value is much larger. A 3.3°C reduction in ECS is simulated, which is also driven by the longwave cloud radiative effects in conjunction with a weaker clear sky shortwave radiative effect which tended to cool the low $p\mathrm{O_2}$ (see also Fig. S6). It should be noted that attempts were made to simulate 2x-experiments for the Wuchiapingian, however what would have been the Wu2x-CM^{10}, in the nomenclature used here, was numerically unstable.

3.4 Earth System Feedbacks

Changes in $p\mathrm{O_2}$ and surface temperatures have the potential to impact the terrestrial carbon cycle by altering the competition between the oxidative and photosynthetic metabolic pathways for Rubisco. Beerling and Berner (2000) simulated significant changes to vegetation productivity in the Permian due to changes in oxygen content. The modelled changes to vegetation in the final 50 years of the Asselian and Wuchiapingian experiments are investigated. Focusing on changes to vegetation across the Permian, the dominant vegetation fractions for As-CM^{35}, As-CM^{10}, Wu-CM^{35} and Wu-CM^{10} are shown in Fig. 10. For low $p\mathrm{CO_2}$ in the Asselian, increasing $p\mathrm{O_2}$ leads to a reduction in the extent of broadleaf trees and greater proliferation of grasses

Clim. Past Discuss., https://doi.org/10.5194/cp-2018-149
Manuscript under review for journal Clim. Past
Discussion started: 14 December 2018

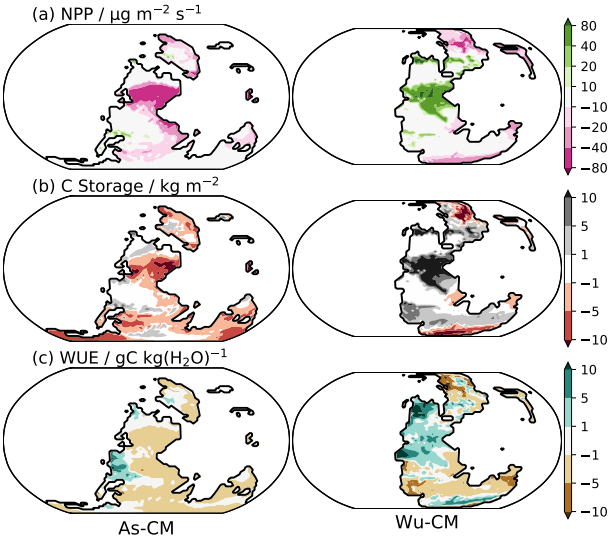

Figure 11. As-CM$^{35}_{10}$ (left) and Wu-CM$^{35}_{10}$ (right) anomalies for (a) net primary productivity, (b) total carbon storage and (c) water use efficiency.

and shrubs. This would be consistent with increases in photorespiration at high pO_2. The reverse is true in the Wuchiapingian simulations with increases in the extent of tropical broadleaf forests. It should be noted that the simulation of plant functional types is carefully tuned to present day vegetation which was likely considerably different in the past. Therefore, caution should be exercised when extrapolating to past vegetation changes.

Figure 11a shows the change in net primary productivity (NPP) for As-CM$^{35}_{10}$ and Wu-CM$^{35}_{10}$. The Asselian simulations shows a large reduction in net primary productivity (NPP) as pO_2 is increased (Figure 11A, –59 $\mathrm{Pg\,C\,yr^{-1}}$) while the reverse is true in the Wuchiapingian simulations (+33 $\mathrm{Pg\,C\,yr^{-1}}$). At low pCO_2, it is expected that competition for Rubisco will be won out by O_2 and therefore that rates of photorespiration should lead to a decline in photosynthesis. This is reflected in the gross primary productivity (GPP, –34 %) and NPP (–52 %) response for the Asselian. During the Wuchiapingian, there may be sufficient CO_2 that competition is much less sensitive to the pO_2 so changes to NPP are much less significant. In fact, NPP is increased by 14 % (GPP +18 %). Tropical water use efficiency is also higher in Wu-CM^{35} (Figure 11c), which suggests that water economy of plants could alter to adapt to a higher pO_2 (Beerling and Berner, 2000).

These net primary productivity changes are reflected in the total carbon storage (Figure 11b) which is lower as pO_2 is increased in As-CM (–338 Pg C) and higher as pO_2 is increased in Wu-CM (+379 Pg C). This is dominated by changes in the tropics (in agreement with Beerling and Berner 2000), where broadleaf trees are more expansive in Wu-CM^{35}. Cooler terrestrial tropical temperatures, particularly in the warm month (Figure 4e) reduces the pO_2 inhibition of Rubisco and reduces the rate of respiration by vegetation and soils (Long, 1991; Beerling and Berner, 2000). The changes in terrestrial carbon storage are equivalent to 56 % of the atmospheric CO_2 content in the Asselian and 16% in the Wuchiapingian which suggests that pO_2 induced Earth system feedbacks could have significant impacts on atmospheric pCO_2. That terrestrial carbon storage increases

Clim. Past Discuss., https://doi.org/10.5194/cp-2018-149
Manuscript under review for journal Clim. Past
Discussion started: 14 December 2018

Climate of the Past Discussions

with pO_2 in the Wuchiapingian simulations suggests that the physical climate response to pO_2 is important for determining the strength of carbon cycle feedbacks in the Permian.

As these simulations are fully coupled and changes to oxygen content affect temperatures, radiation and precipitation it is challenging to explore all the possible contributions to differences between these results and the more idealised Beerling and Berner (2000) simulations. However, there is general agreement that changes occur in the signs of the response of NPP and total carbon storage. This supports the conclusions of Beerling and Berner (2000) that high pO_2 in the early Permian may have played an important role in the evolution of plants. Note that while the atmosphere and vegetation are coupled in the physical sense, the carbon cycle is not interactive.

3.5 Maastrichtian Model-Proxy Comparison

While the changes to global-mean surface temperature (GMST) from changes in pO_2 are less substantial than for large changes in CO_2, regional changes are comparable to other smaller changes which have been widely investigated such as changes to topography or the differences between CO_2 forcing and cloud albedo modification (Carlson and Caballero, 2017). This raises the question whether oxygen content could reasonably alter the agreement between models and proxy data? For this we employ the Maastrichtian experiments as there is a considerable quantity of widely used proxy data for the Maastrichtian (Upchurch et al., 2015). In addition to the Ma-CM^{35}, Ma-CM^{21} and Ma-CM^{10} experiments, further experiments (the Ma2x-CM^{35}* and Ma2x-CM^{10}*) were iterated for 1000 model years and the final 50 years were analysed.

Figure 12a shows the annual mean surface air temperature (SAT) simulated for the Ma-CM^{21} case along with the locations of the proxy data employed for comparison with the model in Fig. 12b. As is commonly observed amongst many climate models, HadCM3-BL struggles to simulate the high latitude warmth indicated by proxy reconstructions. A consideration of the seasonality of the proxies could reconcile some of these differences (Figure 12b, grey vertical bars), however it is likely that a number of factors such as model deficiencies or climate feedbacks such as convective clouds or cloud droplet radius changes may play a role in the shallower equator-to-pole temperature gradient. The normalised mean bias, root mean square error, normalised mean bias factor and normalised mean absolute error factor (Yu et al., 2006) of the Ma-CM^{35}, Ma-CM^{21}, Ma-CM^{10}, Ma2x-CM^{10}* and Ma2x-CM^{35}* experiments are shown in Table 3. These show that across both CO_2 contents that increasing the oxygen content leads to a reduction in all bias metrics against the Upchurch et al. (2015) data, however doubling the CO_2 content led to the largest improvement in bias scores.

3.6 Importance of Wind Stress

Saenko (2009) assessed the contribution of wind stress to global climate in the Canadian Centre for Climate Modeling and Analysis model by setting the wind stress experienced by the ocean to zero and simulated a reduction in global mean surface temperature by 8.7°C. Similar simulations were performed with HadCM3-BL (τPI-CM*, τMa-CM*, τWu-CM* and τAs-CM*) and iterated for 500 model years. This is insufficient to achieve an equilibrium climate response, however as the aim is to investigate the relative magnitude of the changes this was considered adequate to explore this sensitivity study.

Clim. Past Discuss., https://doi.org/10.5194/cp-2018-149
Manuscript under review for journal Clim. Past
Discussion started: 14 December 2018

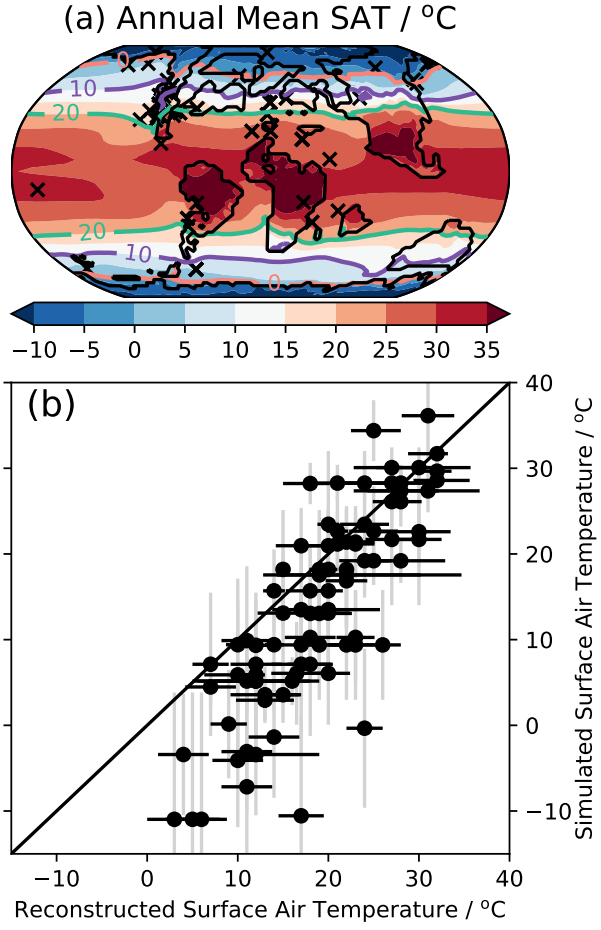

Figure 12. (a) Annual mean surface air temperature in Ma-CM[21]. Contours for 20 °C (green), 10 °C (purple) and 0 °C (orange) are indicated. Proxy data locations are indicated by black crosses. (b) A comparison between proxy reconstructed and Ma-CM[21] simulated annual mean surface air temperature interpolated onto the site location. Errors in the proxy values are taken from Upchurch et al. (2015). The standard deviation of the simulated monthly mean surface air temperature is indicated in light grey as an indication of the seasonality simulated at that site.

The impacts of removing wind stress are shown in Fig. 13. HadCM3-BL simulated a –7.3°C surface air temperature change, slightly weaker than Saenko (2009) however it should be noted that HadCM3-BL was iterated for substantially longer (500 years vs 100 years). τAs-CM* was the most sensitive to the removal of wind stress, with a –15.7°C SAT change. By contrast, the warmest climates showed more muted cooling in response to the removal of wind stress forcing. τMa-CM* shows an SAT anomaly of –2.7°C while τWu-CM* shows an SAT anomaly of –3.51°C. This suggests that the climate response to wind stress changes is likely to depend on the ocean configuration and the background climate – warmer climates of the Wuchiapingian and

Clim. Past Discuss., https://doi.org/10.5194/cp-2018-149
Manuscript under review for journal Clim. Past
Discussion started: 14 December 2018

Climate of the Past Discussions
Open Access
EGU

Table 3. Comparison between the simulated annual mean surface air temperature and the Upchurch et al. (2015) reconstructed surface air temperature. NMB: normalised mean bias. RMSE: root mean square error. NMBF: normalised mean bias factor. NMAEF: normalised mean absolute error factor (Yu et al., 2006). Best performing simulation for a particular metric is indicated in bold.

Experiment	NMB	RMSE / °C	NMBF	NMAEF
Ma-CM^{35}	–0.24	7.92	–0.31	0.41
Ma-CM^{21}	–0.28	8.68	–0.39	0.48
Ma-CM^{10}	–0.28	8.83	–0.40	0.50
Ma2x-CM^{35}*	**–0.04**	**5.82**	**–0.04**	**0.25**
Ma2x-CM^{10}*	+0.07	6.22	+0.07	0.26

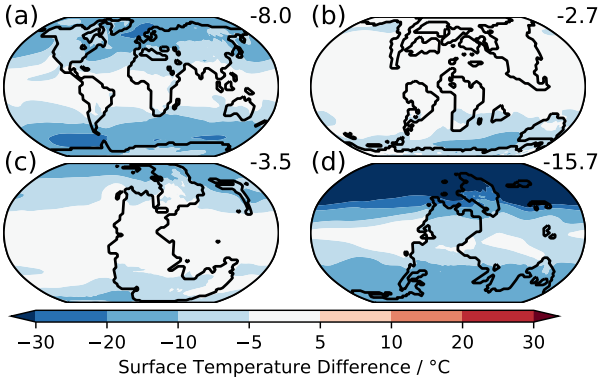

Figure 13. Surface air temperature anomalies for (a) τPI-CM*–PI-CM^{21}, (b) τMa-CM*–Ma-CM^{21}, (c) τWu-CM*–Wu-CM^{21}, (d) τAs-CM*–As-CM^{21}

Maastrichtian appear to be much less sensitive to wind stress forcing. This could be due to the lower meridional temperature gradient.

4 Discussion

Through its impact on atmospheric mass, oxygen content has the capacity to alter the radiative budget of the atmosphere and therefore on Earth's climate. These simulations suggest that the interactions between radiative and dynamical feedbacks lead to some consistent climatic changes in HadCM3-BL with increasing pO_2

- Reduction in the seasonal cycle in surface air temperature.
- Reduction in equator-to-pole temperature gradient.
- Reduction in global precipitation.

Clim. Past Discuss., https://doi.org/10.5194/cp-2018-149
Manuscript under review for journal Clim. Past
Discussion started: 14 December 2018

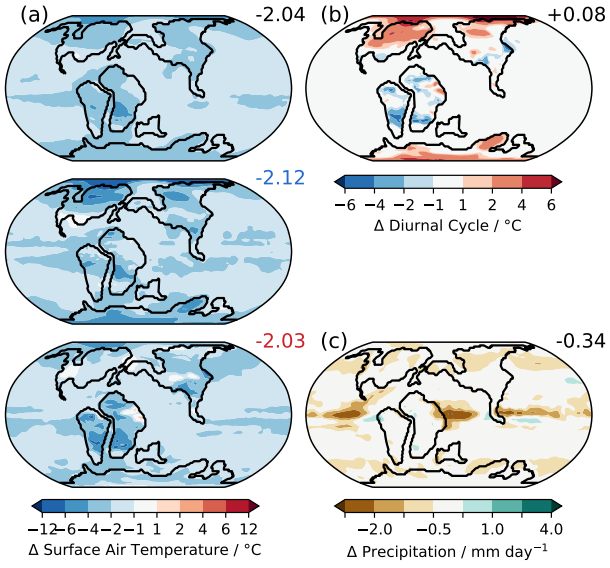

Figure 14. 21 %–10 % O_2 anomalies for Poulsen et al. (2015) simulations. (a) Annual mean, cold month mean and warm month mean surface air temperature difference. (b) Change to diurnal cycle and (c) precipitation.

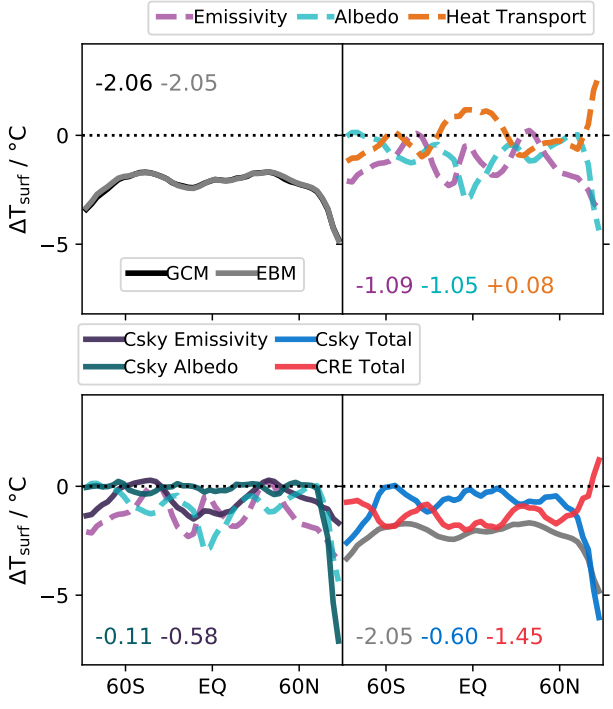

Figure 15. 1D-energy balance decomposition analogous to Fig. 7 for the 21–10 % O_2Poulsen et al. (2015) simulations.

Clim. Past Discuss., https://doi.org/10.5194/cp-2018-149
Manuscript under review for journal Clim. Past
Discussion started: 14 December 2018

HadCM3-BL simulates a reduced equilibrium climate sensitivity due to changes in longwave cloud feedbacks. HadGEM3-AO results also support a reduced sensitivity to CO_2 content at high pO_2. The pre-industrial Holocene results are supported by 1D radiative convective simulations, 2D model simulations and slab ocean 3D model simulations of the Archean. This raises a discrepancy with the Poulsen et al. (2015) study, which simulated a reduction in global mean surface temperature when increasing oxygen content in the GENESIS model. Figure 14a shows the surface air temperature change between the 10 % and 21 % Cenomanian (100.5–93.9 Ma) simulations from the Poulsen et al. (2015) study. These show a –2.04°C change in the annual mean. To understand the mechanisms behind this, we performed the 1D-energy balance decomposition on the Poulsen et al. (2015) Cenomanian 21–10 % model output. The results are shown in Fig. 15. This shows that the cloudy-sky contribution to the temperature change dominates the climate response, contributing –1.45°C. However, the clear sky contribution is also negative (–0.60°C) including both clear-sky emissivity (–0.58°C) and clear-sky albedo (–0.11°C). This appears to support the argument that tropical cloud feedbacks explain the discrepancy between the Poulsen et al. (2015) simulations and results of 1D radiative convective models (Goldblatt, 2016), however this cannot be the only factor. An increase in pressure broadening of absorption lines would be expected to lead to a positive contribution from the clear-sky emissivity. This suggests that cloud feedbacks alone cannot explain the discrepancy and that the implementation of pressure broadening may play a role in the anomalous Poulsen et al. (2015) response. In addition, changes to the seasonal cycle (Figure 14a) simulated by Poulsen et al. (2015) are also inconsistent with the HadGEM-AO and HadCM3-BL results, in which all simulations led to a reduced seasonal cycle as pO_2 increases. The Poulsen et al. (2015) Cenomanian simulations actually simulates a larger seasonal cycle at high pO_2 which is challenging to reconcile with the radiative and physical processes. This change in shortwave-longwave balance could also be evident in the diurnal cycle, which ought to be weaker at high O_2 for the same reasons as the seasonal cycle, however this increases between 10 % and 21 % O_2 in the Poulsen et al. (2015) simulation. Sub-daily data was not available from the HadCM3-BL or HadGEM3-AO simulations for comparison. Note that the Poulsen et al. (2015) simulations were for an earlier Cretaceous period than those performed in HadCM3-BL, the Maastrichtian. However, as Poulsen et al. (2015) employed a slab ocean the heat transport is fixed so ocean heat transport changes caused by changes in continental configuration will not have been simulated.

The simulations presented in here suggest that perturbations to the wind-driven ocean circulation by increasing atmospheric mass leads to warmer temperatures, particularly at high latitudes. The magnitude of the results varies depending on the precise continental configuration and background climate state. Gyre circulations vary between the preindustrial and the Maastrichtian and Asselian case studies. Given the importance of the wind-driven ocean circulation response this suggests that a 3D representation of ocean circulation is necessary in order to capture the temperature response to atmospheric mass changes. It should be noted however that Charnay et al. (2013) simulated higher surface temperatures for the early Earth at high atmospheric mass with a slab ocean model.

The use of 3D oceans is now widespread in the palaeoclimate community, however this is not widely used in the exoplanet/early earth community (e.g. Kilic et al. 2017) and for early Earth studies such as the Archean (e.g. Charnay et al. 2013). While boundary conditions for these studies are sparse or in some cases non-existent the additional uncertainty associated

with using a slab ocean should be considered. AO-GCM studies remain the best way to assess the complex coupling between potentially competing radiative and dynamical effects.

Increased oxygen content may also contribute to explaining the very low temperature gradients for hothouse climates in the Phanerozoic – the "shallow gradients paradox" (Huber and Caballero, 2011). However, there are other mechanisms which could lead to similar changes. Increases in the effective radii of liquid clouds leads to considerable warming, particularly at high latitudes. While the tropics also warm the equator-to-pole temperature gradient is reduced. Abbot and Tziperman (2008) describe a convective cloud feedback which warms the high latitudes, particularly in winter. Upchurch et al. (2015) found that CCSM3 is able to reasonably simulate the shallow Maastrichtian temperature gradient when the effective radii of cloud droplets was set to 17 μm globally (comapred to typical values today around 8 μm over land surfaces and 14 μm over ocean surfaces and 17 μm only observed for the most pristine of clouds in the current atmosphere), however this is hard to reconcile with the high primary productivity likely in hothouse climates and the large contributions of biogenic sources of volatile organic compounds and ammonia in the pre-industrial atmosphere (Gordon et al., 2017). In addition, the seasonality of cloud droplet changes is likely to lead to the strongest temperature changes in the warm months which may increase lead to unreasonably high temperature changes in the tropics.

One criticism of high oxygen variability in the Phanerozoic is the possibility of runaway fire at high oxygen contents (Watson et al., 1978). While subsequent experiments have put this in doubt, fire is undoubtedly a negative feedback on oxygen content. However, the cooling of warmest month temperatures over tropical and midlatitude continents in Wu-CM[35] may provide somewhat of a protective mechanism against runaway fire regimes taking hold. Lightning is a major cause of paleofire (Scott and Jones, 1994) so the reduction in convection at high pO_2 would also lead to fewer lightning strikes which would reduce fire initiation. In addition, higher fire risk could have favoured the evolution and spread of more fire-resistant species (Robinson, 1990).

The simulations of Permian climate (As-CM and Wu-CM) also suggest a strong role for pO_2 variability in the terrestrial carbon cycle. However, there are many limitations to the modelling approach employed here. The plant functional types employed here are the same as present day. In particular, C_4 photosynthesis likely evolved in the Oligocene (Sage, 2004) although there is evidence of vegetation which causes C_4-like fractionation, suggesting different vegetation adaptations operating in the past (Jones, 1994). In addition, angiosperms did not evolve until the Cretaceous so gymnosperms such as cycads were more widespread in the Permian (Taylor et al., 2009). TRIFFID and other dynamic plant models were not developed with these changes in plant types in mind so simulating past vegetation changes is still a considerable challenge. However, scientific understanding of the role of plants in the climate in the Paleozoic is still immature. While early evidence suggested that late Paleozoic vegetation was unproductive based on analysis of the closest modern relatives, this perspective is increasingly being challenged (Wilson et al., 2017). Other approaches such as trait based methods (Van Bodegom et al., 2012) may be able to achieve more insights into the role of pO_2 in the Earth system. We also have not accounted for changes to the ocean carbon cycle. A biogeochemical model study suggests that pervasive oceanic anoxia and euxinia only occur below an oxygen level of around 10 % (Ozaki and Tajika, 2013) which may be below the fire threshold (Belcher et al., 2010) and therefore not of

Clim. Past Discuss., https://doi.org/10.5194/cp-2018-149
Manuscript under review for journal Clim. Past
Discussion started: 14 December 2018

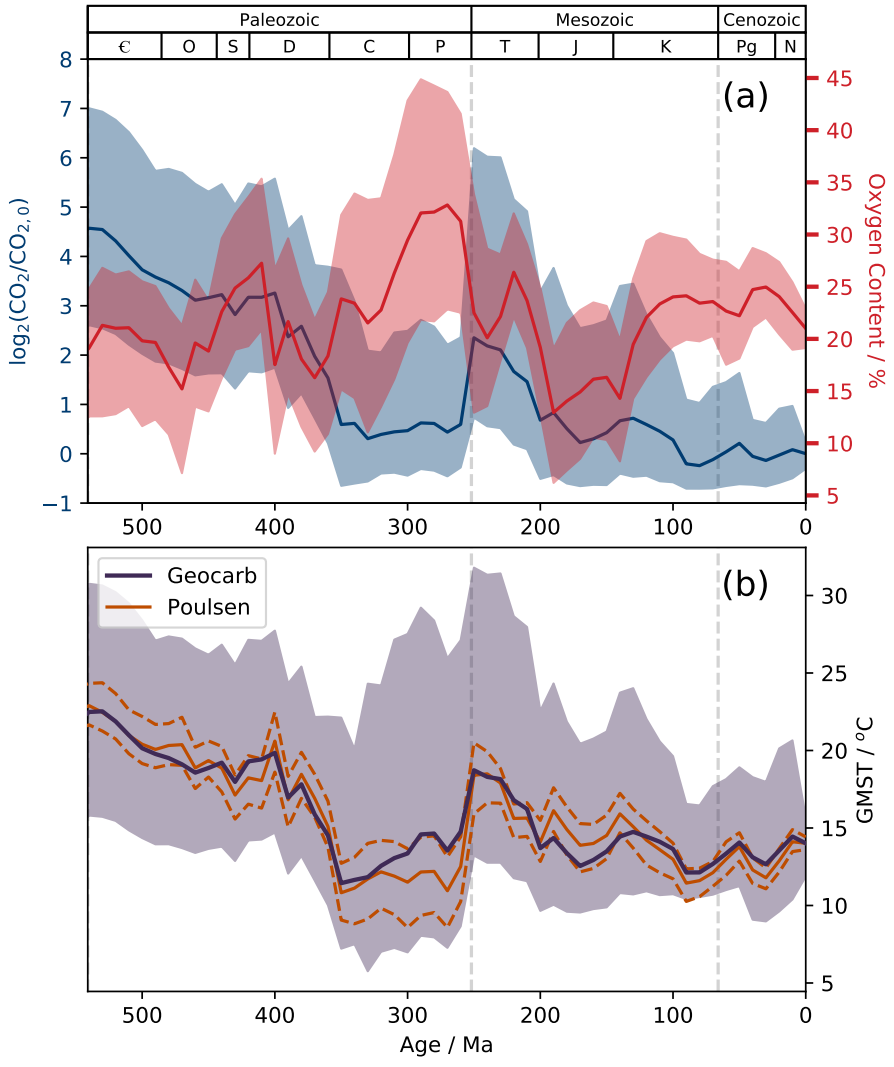

Figure 16. (a) Reconstructed CO_2 (doublings from Pleistocene values, blue) and O_2 content (red) and 95% confidence intervals (shading) from Royer et al. (2014) Geocarb simulations. (b) GMST reconstructed using Geocarb pCO_2 and climate sensitivity values (purple) and the uncertainty in GMST from pCO_2 uncertainty (purple shading). GMST reconstructed, accounting for pO_2 according to Poulsen et al. (2015) global mean temperature sensitivities (solid orange) and the uncertainty due to Geocarb pO_2 (orange dashed).

relevance to many periods in the Phanerozoic. However, the extent of oceanic anoxic events may be sensitive to atmospheric pO_2 (Clarkson et al., 2018).

Given the relatively small contribution of O_2 to improving the proxy-model agreement for the Maastrichtian at the largest oxygen changes and the small changes in global mean surface temperature (GMST, 1.5 °C maximum) compared to ECS (~3 °C), this raises the question of how much pO_2 variability contributes to uncertainty in Phanerozoic surface temperature

Clim. Past Discuss., https://doi.org/10.5194/cp-2018-149
Manuscript under review for journal Clim. Past
Discussion started: 14 December 2018

even with such large uncertainties in pO_2 reconstructions. Figure 16 shows reconstructed Phanerozoic surface temperatures based on CO_2 content and climate sensitivity from the Geocarb model (purple, Royer et al. 2014). The uncertainty associated with the 95% confidence interval in simulated pCO_2 is also indicated (purple shading). Analysis of the Poulsen et al. (2015) simulations suggests a global mean surface temperature reduction of 0.21 °C per percentage increase in O_2. Accounting for the pO_2 simulated by Royer et al. (2014) leads to a mean absolute difference in global mean surface temperature of 0.80 °C and maximum absolute difference of 2.59 °C (Figure 16 orange line). The largest deviations from the Geocarb values occur during the largest deviations from PAL O_2 during the Permian. However, pO_2 contributes little to the uncertainty in reconstruction of global mean surface temperature compared to pCO_2 (Figure 16 orange dashed lines), even if the temperature changes simulated by Poulsen et al. (2015) are reasonable. The HadGEM3-AO and HadCM3-BL simulations show even less sensitivity of global mean surface temperature to pO_2 changes which suggests this is likely an overestimate.

pO_2 therefore remains a secondary contribution to climatic variability in the Phanerozoic but most likely to be important during the Permian. The Artinskian (early Permian, 283.5–290.1 Ma) is associated with a rapid increase in CO_2 content from ~500 to ~3500 ppmv which is associated with considerable restructuring of tropical vegetation (Montañez et al., 2007). The results in this study suggest that pO_2 variability could have modulated the climate and terrestrial vegetation response to this increase in CO_2 content. Feulner (2017) suggested that Earth was close to entering a Snowball Earth in the late Carboniferous, when pO_2 were higher than today. We hypothesise that the carbon cycle and physical climate feedbacks described in this paper would strongly mitigate against this. If pCO_2 and pO_2 are intimately linked such that cooler climates tends to increase pO_2 this would suggest that pO_2 responses have helped to prevent Snowball Earth initiation in the Phanerozoic.

5 Conclusions

The numerical simulations performed in this study reconcile the surface temperature response to oxygen content changes across the hierarchy of model complexity:

- Under pre-industrial Holocene conditions, increasing atmospheric pO_2 leads to an increase in global-mean surface temperature in agreement with 1D radiative-convective model simulations. This increase is greater in the cold-month mean than the warm month-mean. The equator-to-pole temperature gradient is reduced, particularly in the cold-month mean, consistent with a stronger greenhouse effect at high atmospheric pressure.
- Lower incident surface shortwave radiation leads to a slow down of the hydrological cycle. Precipitation decreases globally under high pO_2, with regional variations.
- The climate sensitivity is lower at high pO_2, particularly in the Maastrichtian. This appears to reconcile the results of the 1D and 3D modelling approaches.
- For the Maastrichtian, model-proxy agreement is stronger at high pO_2 irrespective of pCO_2. Both simulations at 112 Pa CO_2 agree better with the Upchurch et al. (2015) proxy reconstruction than those at 56 Pa CO_2.

- The climate response simulated by Poulsen et al. (2015) is inconsistent with the radiative changes when considering a 1D-energy balance model decomposition of the surface temperature changes. Tropical cloud feedbacks alone were not sufficient to explain the discrepancy.
- The climate response to oxygen content variability is state-dependent so should be considered on a case-by-case basis. However, the changes are relatively small compared to the role of CO_2 in the Phanerozoic (Royer et al., 2014).

Code and data availability. Processed model output and analysis scripts will be made available on the NERC data centre. The Met Office Unified Model is available for use under licence. Please see http://www.metoffice.gov.uk/research/modelling-systems/unified-model for more information. The ocean bathymetry and land orography reconstructions are ©Getech.

Competing interests. The authors declare no competing interests.

Acknowledgements. DCW acknowledges support from a UK Natural Environment Research Council Doctoral Training Program studentship (Ref 1502139). This work was carried out using the computational facilities of the Advanced Computing Research Centre, University of Bristol http://www.bris.ac.uk/acrc/. We acknowledge use of the MONSooN system, a collaborative facility supplied under the Joint Weather and Climate Research Programme, a strategic partnership between the Met Office and the Natural Environment Research Council. DCW acknowledges Eric Wolff and David Stevenson for their comments on the PhD thesis from which this paper largely forms a part.

References

Abbot, D. S. and Tziperman, E.: A high-latitude convective cloud feedback and equable climates, Quarterly Journal of the Royal Meteorological Society, 134, 165–185, https://doi.org/10.1002/qj.211, 2008.

Algeo, T. J. and Ingall, E.: Sedimentary Corg:P ratios, paleocean ventilation, and Phanerozoic atmospheric pO_2, Palaeogeography, Palaeoclimatology, Palaeoecology, 256, 130–155, https://doi.org/10.1016/J.PALAEO.2007.02.029, 2007.

Armour, K. C., Bitz, C. M., and Roe, G. H.: Time-Varying Climate Sensitivity from Regional Feedbacks, Journal of Climate, 26, 4518–4534, https://doi.org/10.1175/JCLI-D-12-00544.1, 2013.

Arvidson, R. S., Mackenzie, F. T., and Guidry, M. W.: Geologic history of seawater: A MAGic approach to carbon chemistry and ocean ventilation, Chemical Geology, 362, 287–304, https://doi.org/10.1016/J.CHEMGEO.2013.10.012, 2013.

Awakawa, A. and Lamb, V. R.: Computational Design of the Basic Dynamical Processes of the UCLA General Circulation Model, Methods in Computational Physics: Advances in Research and Applications, 17, 173–265, 1977.

Banerjee, A., Archibald, A. T., Maycock, A., Telford, P., Abraham, N. L., Yang, X., Braesicke, P., and Pyle, J. A.: Lightning NOx, a key chemistry–climate interaction: impacts of future climate change and consequences for tropospheric oxidising capacity, Atmospheric Chemistry and Physics Discussions, 14, 8753–8778, https://doi.org/10.5194/acpd-14-8753-2014, 2014.

Beerling, D., Lake, J., Berner, R., Hickey, L., Taylor, D., and Royer, D.: Carbon isotope evidence implying high O_2/CO_2 ratios in the Permo-Carboniferous atmosphere, Geochimica et Cosmochimica Acta, 66, 3757–3767, https://doi.org/10.1016/S0016-7037(02)00901-8, 2002.

Beerling, D., Berner, R. A., Mackenzie, F. T., Harfoot, M. B., and Pyle, J. A.: Methane and the CH_4-related greenhouse effect over the past 400 million years, American Journal of Science, 309, 97–113, https://doi.org/10.2475/02.2009.01, 2009.

Beerling, D. J. and Berner, R. A.: Impact of a Permo-Carboniferous high O_2 event on the terrestrial carbon cycle., Proceedings of the National Academy of Sciences of the United States of America, 97, 12 428–32, https://doi.org/10.1073/pnas.220280097, 2000.

Beerling, D. J., Fox, A., Stevenson, D. S., and Valdes, P. J.: Enhanced chemistry-climate feedbacks in past greenhouse worlds., Proceedings of the National Academy of Sciences of the United States of America, 108, 9770–9775, https://doi.org/10.1073/pnas.1102409108, 2011.

Belcher, C. M. and McElwain, J. C.: Limits for Combustion in Low O_2 Redefine Paleoatmospheric Predictions for the Mesozoic, Science, 321, 1197–200, 2008.

Belcher, C. M., Yearsley, J. M., Hadden, R. M., McElwain, J. C., and Rein, G.: Baseline intrinsic flammability of Earth's ecosystems estimated from paleoatmospheric oxygen over the past 350 million years., Proceedings of the National Academy of Sciences of the United States of America, 107, 22 448–53, https://doi.org/10.1073/pnas.1011974107, 2010.

Bergman, N. M., Lenton, T. M., and Watson, A. J.: COPSE: A new model of biogeochemical cycling over Phanerozoic time, American Journal of Science, 304, 397–437, https://doi.org/10.2475/ajs.304.5.397, 2004.

Berner, R. A.: Phanerozoic atmospheric oxygen: New results using the GEOCARBSULF model, American Journal of Science, 309, 603–606, https://doi.org/10.2475/07.2009.03, 2009.

Berner, R. A. and Canfield, D. E.: A new model for atmospheric oxygen over Phanerozoic time, American Journal of Science, 289, 333–361, https://doi.org/10.2475/ajs.289.4.333, 1989.

Berner, R. A., Vandenbrooks, J. M., and Ward, P. D.: Evolution. Oxygen and evolution., Science, 316, 557–8, https://doi.org/10.1126/science.1140273, 2007.

Bony, S., Stevens, B., Frierson, D. M. W., Jakob, C., Kageyama, M., Pincus, R., Shepherd, T. G., Sherwood, S. C., Siebesma, A. P., Sobel, A. H., Watanabe, M., and Webb, M. J.: Clouds, circulation and climate sensitivity, Nature Geoscience, 8, 261–268, https://doi.org/10.1038/ngeo2398, 2015.

Brand, U., Posenato, R., Came, R., Affek, H., Angiolini, L., Azmy, K., and Farabegoli, E.: The end-Permian mass extinction: A rapid volcanic CO_2 and CH_4-climatic catastrophe, Chemical Geology, 322-323, 121–144, 2012.

Breecker, D. O., Sharp, Z. D., and McFadden, L. D.: Atmospheric CO_2 concentrations during ancient greenhouse climates were similar to those predicted for A.D. 2100., Proceedings of the National Academy of Sciences of the United States of America, 107, 576–80, https://doi.org/10.1073/pnas.0902323106, 2010.

Budyko, M. I.: The effect of solar radiation variations on the climate of the Earth, Tellus, 21, 611–619, https://doi.org/10.3402/tellusa.v21i5.10109, 1969.

Caballero, R. and Huber, M.: State-dependent climate sensitivity in past warm climates and its implications for future climate projections, Proceedings of the National Academy of Sciences, 110, 14 162–14 167, https://doi.org/10.1073/pnas.1303365110, 2013.

Carlson, H. and Caballero, R.: Atmospheric circulation and hydroclimate impacts of alternative warming scenarios for the Eocene, Climate of the Past, 13, 1037–1048, https://doi.org/10.5194/cp-13-1037-2017, 2017.

Catling, D. C. and Claire, M. W.: How Earth's atmosphere evolved to an oxic state: A status report, Earth and Planetary Science Letters, 237, 1–20, https://doi.org/10.1016/J.EPSL.2005.06.013, 2005.

Catling, D. C., Glein, C. R., Zahnle, K. J., and McKay, C. P.: Why O_2 Is Required by Complex Life on Habitable Planets and the Concept of Planetary "Oxygenation Time", Astrobiology, 5, 415–438, https://doi.org/10.1089/ast.2005.5.415, 2005.

Charnay, B., Forget, F., Wordsworth, R., Leconte, J., Millour, E., Codron, F., and Spiga, A.: Exploring the faint young Sun problem and the possible climates of the Archean Earth with a 3-D GCM, Journal of Geophysical Research: Atmospheres, 118, 10,414–10,431, https://doi.org/10.1002/jgrd.50808, 2013.

Chemke, R., Kaspi, Y., and Halevy, I.: The thermodynamic effect of atmospheric mass on early Earth's temperature, Geophysical Research Letters, 43, 11,414–11,422, https://doi.org/10.1002/2016GL071279, 2016.

Clarkson, M. O., Stirling, C. H., Jenkyns, H. C., Dickson, A. J., Porcelli, D., Moy, C. M., Pogge von Strandmann, P. A. E., Cooke, I. R., and Lenton, T. M.: Uranium isotope evidence for two episodes of deoxygenation during Oceanic Anoxic Event 2., Proceedings of the National Academy of Sciences of the United States of America, 115, 2918–2923, https://doi.org/10.1073/pnas.1715278115, 2018.

Cox, P.: A primitive equation, 3-dimensional model of the ocean, GFDL Ocean Group Technical Report No. 1, Tech. rep., Geophysical Fluid Dynamics Laboratory, Princeton, New Jersey, 1984.

Cox, P., Huntingford, C., and Harding, R.: A canopy conductance and photosynthesis model for use in a GCM land surface scheme, Journal of Hydrology, 212-213, 79–94, https://doi.org/10.1016/S0022-1694(98)00203-0, 1998.

Cox, P., Betts, R. A., Jones, C., A. Spall, S., and J. Totterdell, I.: Acceleration of global warming due to carbon-cycle feedbacks in a coupled model, Nature, 408, 184–187, 2000.

Cox, P. M., Betts, R. A., Bunton, C. B., Essery, R. L. H., Rowntree, P. R., and Smith, J.: The impact of new land surface physics on the GCM simulation of climate and climate sensitivity, Climate Dynamics, 15, 183–203, https://doi.org/10.1007/s003820050276, 1999.

Davies, T., Cullen, M. J. P., Malcolm, A. J., Mawson, M. H., Staniforth, A., White, A. A., and Wood, N.: A new dynamical core for the Met Office's global and regional modelling of the atmosphere, Quarterly Journal of the Royal Meteorological Society, 131, 1759–1782, https://doi.org/10.1256/qj.04.101, 2005.

Dwyer, J. G., Biasutti, M., and Sobel, A. H.: Projected Changes in the Seasonal Cycle of Surface Temperature, Journal of Climate, 25, 6359–6374, https://doi.org/10.1175/JCLI-D-11-00741.1, 2012.

Edwards, C. T., Saltzman, M. R., Royer, D. L., and Fike, D. A.: Oxygenation as a driver of the Great Ordovician Biodiversification Event, Nature Geoscience, 10, 925–929, https://doi.org/10.1038/s41561-017-0006-3, 2017.

Edwards, J. M. and Slingo, A.: Studies with a flexible new radiation code. I: Choosing a configuration for a large-scale model, Quarterly Journal of the Royal Meteorological Society, 122, 689–719, https://doi.org/10.1002/qj.49712253107, 1996.

Essery, R. L. H., Best, M. J., Betts, R. A., Cox, P. M., Taylor, C. M., Essery, R. L. H., Best, M. J., Betts, R. A., Cox, P. M., and Taylor, C. M.: Explicit Representation of Subgrid Heterogeneity in a GCM Land Surface Scheme, Journal of Hydrometeorology, 4, 530–543, https://doi.org/10.1175/1525-7541(2003)004<0530:EROSHI>2.0.CO;2, 2003.

Falkowski, P. G., Katz, M. E., Milligan, A. J., Fennel, K., Cramer, B. S., Aubry, M. P., Berner, R. A., Novacek, M. J., and Zapol, W. M.: The Rise of Oxygen over the Past 205 Million Years and the Evolution of Large Placental Mammals, Science, 309, 2005.

Feulner, G.: The faint young Sun problem, Reviews of Geophysics, 50, RG2006, https://doi.org/10.1029/2011RG000375, 2012.

Feulner, G.: Formation of most of our coal brought Earth close to global glaciation., Proceedings of the National Academy of Sciences of the United States of America, 114, 11 333–11 337, https://doi.org/10.1073/pnas.1712062114, 2017.

Finney, D. L., Doherty, R. M., Wild, O., Stevenson, D. S., MacKenzie, I. A., and Blyth, A. M.: A projected decrease in lightning under climate change, Nature Climate Change, 8, 210–213, https://doi.org/10.1038/s41558-018-0072-6, 2018.

Forster, P. M. and Shine, K. P.: Radiative forcing and temperature trends from stratospheric ozone changes, Journal of Geophysical Research: Atmospheres, 102, 10 841–10 855, https://doi.org/10.1029/96JD03510, 1997.

Franks, P. J., Royer, D. L., Beerling, D. J., Van de Water, P. K., Cantrill, D. J., Barbour, M. M., and Berry, J. A.: New constraints on atmospheric CO_2 concentration for the Phanerozoic, Geophysical Research Letters, 41, 4685–4694, 2014.

Glasspool, I. J. and Scott, A. C.: Phanerozoic concentrations of atmospheric oxygen reconstructed from sedimentary charcoal, Nature Geoscience, 3, 627–630, https://doi.org/10.1038/ngeo923, 2010.

Goldblatt, C.: Comment on "Long-term climate forcing by atmospheric oxygen concentrations", Science, 353, 132, 2016.

Goldblatt, C., Claire, M. W., Lenton, T. M., Matthews, A. J., Watson, A. J., and Zahnle, K. J.: Nitrogen-enhanced greenhouse warming on early Earth, Nature Geoscience, 2, 891–896, https://doi.org/10.1038/ngeo692, 2009.

Gordon, C., Cooper, C., Senior, C. A., Banks, H., Gregory, J. M., Johns, T. C., Mitchell, J. F. B., and Wood, R. A.: The simulation of SST, sea ice extents and ocean heat transports in a version of the Hadley Centre coupled model without flux adjustments, Climate Dynamics, 16, 147–168, https://doi.org/10.1007/s003820050010, 2000.

Gordon, H., Kirkby, J., Baltensperger, U., Bianchi, F., Breitenlechner, M., Curtius, J., Dias, A., Dommen, J., Donahue, N. M., Dunne, E. M., Duplissy, J., Ehrhart, S., Flagan, R. C., Frege, C., Fuchs, C., Hansel, A., Hoyle, C. R., Kulmala, M., Kürten, A., Lehtipalo, K., Makhmutov, V., Molteni, U., Rissanen, M. P., Stozkhov, Y., Tröstl, J., Tsagkogeorgas, G., Wagner, R., Williamson, C., Wimmer, D., Winkler, P. M., Yan, C., and Carslaw, K. S.: Causes and importance of new particle formation in the present-day and preindustrial atmospheres, Journal of Geophysical Research: Atmospheres, 122, 8739–8760, https://doi.org/10.1002/2017JD026844, 2017.

Gregory, J. M., Ingram, W. J., Palmer, M. A., Jones, G. S., Stott, P. A., Thorpe, R. B., Lowe, J. A., Johns, T. C., and Williams, K. D.: A new method for diagnosing radiative forcing and climate sensitivity, Geophysical Research Letters, 31, L03 205, https://doi.org/10.1029/2003GL018747, 2004.

Hadjinicolaou, P. and Pyle, J. A.: The Impact of Arctic Ozone Depletion on Northern Middle Latitudes: Interannual Variability and Dynamical Control, Journal of Atmospheric Chemistry, 47, 25–43, https://doi.org/10.1023/B:JOCH.0000012242.06578.6c, 2004.

Hagemann, M., Weber, A. P., and Eisenhut, M.: Photorespiration: origins and metabolic integration in interacting compartments, Journal of Experimental Botany, 67, 2915–2918, https://doi.org/10.1093/jxb/erw178, 2016.

Haigh, J. D. and Pyle, J. A.: Ozone perturbation experiments in a two-dimensional circulation model, Quarterly Journal of the Royal Meteorological Society, 108, 551–574, https://doi.org/10.1002/qj.49710845705, 1982.

Hansen, K. W. and Wallmann, K.: Cretaceous and Cenozoic evolution of seawater composition, atmospheric O_2 and CO_2: A model perspective, American Journal of Science, 303, 94–148, https://doi.org/10.2475/ajs.303.2.94, 2003.

Harfoot, M. B. J., Beerling, D. J., Lomax, B. H., and Pyle, J. a.: A two-dimensional atmospheric chemistry modeling investigation of Earth's Phanerozoic O_3 and near-surface ultraviolet radiation history, Journal of Geophysical Research: Atmospheres, 112, D07 308, https://doi.org/10.1029/2006JD007372, 2007.

He, T., Pausas, J. G., Belcher, C. M., Schwilk, D. W., and Lamont, B. B.: Fire-adapted traits of *Pinus* arose in the fiery Cretaceous, New Phytologist, 194, 751–759, 2012.

Heinemann, M.: Warm and sensitive Paleocene-Eocene Climate, Ph.D. thesis, Universität Hamburg, 2009.

Heinemann, M., Jungclaus, J. H., and Marotzke, J.: Warm Paleocene/Eocene climate as simulated in ECHAM5/MPI-OM, Climate of the Past, 5, 1297–1336, https://doi.org/10.5194/cpd-5-1297-2009, http://www.clim-past.net/5/785/2009/cp-5-785-2009.html, 2009.

Hewitt, H. T., Copsey, D., Culverwell, I. D., Harris, C. M., Hill, R. S. R., Keen, A. B., McLaren, A. J., and Hunke, E. C.: Design and implementation of the infrastructure of HadGEM3: The next-generation Met Office climate modelling system, Geoscientific Model Development, 4, 223–253, https://doi.org/10.5194/gmd-4-223-2011, 2011.

Huber, M. and Caballero, R.: The early Eocene equable climate problem revisited, Climate of the Past, 7, 603–633, https://doi.org/10.5194/cp-7-603-2011, 2011.

Hunke, E. and Lipscomb, W.: The Los Alamos sea ice model documentation and software user's manual, Version 4.0, LA-CC-06-012., Tech. rep., Los Alamos National Laboratory,, 2008.

Irvine, P. J., Kravitz, B., Lawrence, M. G., and Muri, H.: An overview of the Earth system science of solar geoengineering, Wiley Interdisciplinary Reviews: Climate Change, 7, 815–833, https://doi.org/10.1002/wcc.423, 2016.

Jones, T. P.: ^{13}C enriched Lower Carboniferous fossil plants from Donegal, Ireland: carbon isotope constraints on taphonomy, diagenesis and palaeoenvironment, Review of Palaeobotany and Palynology, 81, 53–64, https://doi.org/10.1016/0034-6667(94)90126-0, 1994.

Jordan, D. B. and Ogren, W. L.: The CO_2/O_2 specificity of ribulose 1,5-bisphosphate carboxylase/oxygenase, Planta, 161, 308–313, https://doi.org/10.1007/BF00398720, 1984.

Kasting, J. F., Liu, S. C., and Donahue, T. M.: Oxygen levels in the prebiological atmosphere, Journal of Geophysical Research, 84, 3097, https://doi.org/10.1029/JC084iC06p03097, 1979.

Kiehl, J. T. and Shields, C. A.: Sensitivity of the Palaeocene-Eocene Thermal Maximum climate to cloud properties, Philosophical Transactions of the Royal Society A: Mathematical, Physical and Engineering Sciences, 371, 20130 093, https://doi.org/10.1098/rsta.2013.0093, 2013.

Kilic, C., Raible, C. C., and Stocker, T. F.: Multiple Climate States of Habitable Exoplanets: The Role of Obliquity and Irradiance, The Astrophysical Journal, 844, 147, https://doi.org/10.3847/1538-4357/aa7a03, 2017.

Lenton, T. M., Crouch, M., Johnson, M., Pires, N., and Dolan, L.: First plants cooled the Ordovician, Nature Geoscience, 5, 86–89, https://doi.org/10.1038/ngeo1390, 2012.

Li, C., von Storch, J.-S., and Marotzke, J.: Deep-ocean heat uptake and equilibrium climate response, Climate Dynamics, 40, 1071–1086, https://doi.org/10.1007/s00382-012-1350-z, 2013.

Li, J. and Sharma, A.: Evaluation of volcanic aerosol impacts on atmospheric water vapor using CMIP3 and CMIP5 simulations, Journal of Geophysical Research: Atmospheres, 118, 4448–4457, https://doi.org/10.1002/jgrd.50420, 2013.

Long, S. P.: Modification of the response of photosynthetic productivity to rising temperature by atmospheric CO_2 concentrations: Has its importance been underestimated?, Plant, Cell and Environment, 14, 729–739, https://doi.org/10.1111/j.1365-3040.1991.tb01439.x, 1991.

Lunt, D. J., Farnsworth, A., Loptson, C., Foster, G. L., Markwick, P., O'Brien, C. L., Pancost, R. D., Robinson, S. A., and Wrobel, N.: Palaeogeographic controls on climate and proxy interpretation, Climate of the Past, 12, 1181–1198, 2016.

Madec, G.: NEMO ocean engine, Note du Pôle de modélisation, Institut Pierre-Simon Laplace (IPSL), France, No 27, ISSN No 1288-1619, 2008.

Meraner, K., Mauritsen, T., and Voigt, A.: Robust increase in equilibrium climate sensitivity under global warming, Geophysical Research Letters, 40, 5944–5948, 2013.

Mills, B. J., Belcher, C. M., Lenton, T. M., and Newton, R. J.: A modeling case for high atmospheric oxygen concentrations during the Mesozoic and Cenozoic, Geology, 44, 1023–1026, https://doi.org/10.1130/G38231.1, 2016.

Montañez, I. P., Tabor, N. J., Niemeier, D., Dimichele, W. A., Frank, T. D., Fielding, C. R., Isbell, J. L., Birgenheier, L. P., and Rygel, M. C.: CO_2-forced climate and vegetation instability during Late Paleozoic deglaciation., Science, 315, 87–91, https://doi.org/10.1126/science.1134207, 2007.

Nowack, P. J., Luke Abraham, N., Maycock, A. C., Braesicke, P., Gregory, J. M., Joshi, M. M., Osprey, A., and Pyle, J. A.: A large ozone-circulation feedback and its implications for global warming assessments, Nature Climate Change, 5, 41–45, https://doi.org/10.1038/nclimate2451, 2014.

Ozaki, K. and Tajika, E.: Biogeochemical effects of atmospheric oxygen concentration, phosphorus weathering, and sea-level stand on oceanic redox chemistry: Implications for greenhouse climates, Earth and Planetary Science Letters, 373, 129–139, https://doi.org/10.1016/J.EPSL.2013.04.029, 2013.

Payne, R. C., Britt, A. V., Chen, H., Kasting, J. F., and Catling, D. C.: The Response of Phanerozoic Surface Temperature to Variations in Atmospheric Oxygen Concentration, Journal of Geophysical Research: Atmospheres, pp. 10 089–10 096, https://doi.org/10.1002/2016JD025459, 2016.

Pope, V. D., Gallani, M. L., Rowntree, P. R., and Stratton, R. A.: The impact of new physical parametrizations in the Hadley Centre climate model: HadAM3, Climate Dynamics, 16, 123–146, https://doi.org/10.1007/s003820050009, 2000.

Poulsen, C. J., Tabor, C., and White, J. D.: Long-term climate forcing by atmospheric oxygen concentrations, Science, 348, 1238–41, 2015.

Rasulov, B., Hüve, K., Välbe, M., Laisk, A., and Niinemets, U.: Evidence that light, carbon dioxide, and oxygen dependencies of leaf isoprene emission are driven by energy status in hybrid aspen., Plant physiology, 151, 448–60, https://doi.org/10.1104/pp.109.141978, 2009.

Robinson, J.: Phanerozoic O_2 variation, fire, and terrestrial ecology, Palaeogeography, Palaeoclimatology, Palaeoecology, 75, 223–240, https://doi.org/10.1016/0031-0182(89)90178-8, 1989.

Robinson, J. M.: Lignin, land plants, and fungi: Biological evolution affecting Phanerozoic oxygen balance, Geology, 18, 607, https://doi.org/10.1130/0091-7613(1990)018<0607:LLPAFB>2.3.CO;2, 1990.

Royer, D., Berner, R., Montañez, I., and Tabor, N.: CO_2 as a primary driver of Phanerozoic climate, GSA today, 14, 4–10, 2004.

Royer, D. L.: Climate Sensitivity in the Geologic Past, Annual Review of Earth and Planetary Sciences, 44, 277–293, 2016.

Royer, D. L., Donnadieu, Y., Park, J., Kowalczyk, J., and Godderis, Y.: Error analysis of CO_2 and O_2 estimates from the long-term geochemical model GEOCARBSULF, American Journal of Science, 314, 1259–1283, https://doi.org/10.2475/09.2014.01, 2014.

Saenko, O. A.: On the Climatic Impact of Wind Stress, Journal of Physical Oceanography, 39, 89–106, https://doi.org/10.1175/2008JPO3981.1, 2009.

Sage, R. F.: The evolution of C_4 photosynthesis, New Phytologist, 161, 341–370, https://doi.org/10.1111/j.1469-8137.2004.00974.x, 2004.

Saltzman, M. R., Young, S. A., Kump, L. R., Gill, B. C., Lyons, T. W., and Runnegar, B.: Pulse of atmospheric oxygen during the late Cambrian., Proceedings of the National Academy of Sciences of the United States of America, 108, 3876–81, https://doi.org/10.1073/pnas.1011836108, 2011.

Savitzky, A. and Golay, M. J. E.: Smoothing and Differentiation of Data by Simplified Least Squares Procedures., Analytical Chemistry, 36, 1627–1639, https://doi.org/10.1021/ac60214a047, 1964.

Scott, A. C. and Glasspool, I. J.: The diversification of Paleozoic fire systems and fluctuations in atmospheric oxygen concentration., Proceedings of the National Academy of Sciences of the United States of America, 103, 10 861–5, https://doi.org/10.1073/pnas.0604090103, 2006.

Scott, A. C. and Jones, T. P.: The nature and influence of fire in Carboniferous ecosystems, Palaeogeography, Palaeoclimatology, Palaeoecology, 106, 91–112, https://doi.org/10.1016/0031-0182(94)90005-1, 1994.

Sellers, W. D.: A Global Climatic Model Based on the Energy Balance of the Earth-Atmosphere System, Journal of Applied Meteorology, 8, 392–400, https://doi.org/10.1175/1520-0450(1969)008<0392:AGCMBO>2.0.CO;2, 1969.

Simmons, A. J. and Strüfing, R.: Numerical forecasts of stratospheric warming events using a model with a hybrid vertical coordinate, Quarterly Journal of the Royal Meteorological Society, 109, 81–111, https://doi.org/10.1002/qj.49710945905, 1983.

Smith, B. N.: Evolution of C4 photosynthesis in response to changes in carbon and oxygen concentrations in the atmosphere through time, Biosystems, 8, 24–32, https://doi.org/10.1016/0303-2647(76)90004-6, 1976.

Steinthorsdottir, M. and Pole, M.: Global trends of pCO_2 across the Cretaceous–Paleogene boundary supported by the first Southern Hemisphere stomatal proxy-based pCO_2 reconstruction, Palaeogeography, Palaeoclimatology, Palaeoecology, 464, 143–152, https://doi.org/10.1016/J.PALAEO.2016.04.033, 2016.

Stolper, D. A., Bender, M. L., Dreyfus, G. B., Yan, Y., and Higgins, J. A.: A Pleistocene ice core record of atmospheric O2 concentrations., Science, 353, 1427–1430, https://doi.org/10.1126/science.aaf5445, 2016.

Tappert, R., McKellar, R. C., Wolfe, A. P., Tappert, M. C., Ortega-Blanco, J., and Muehlenbachs, K.: Stable carbon isotopes of C3 plant resins and ambers record changes in atmospheric oxygen since the Triassic, Geochimica et Cosmochimica Acta, 121, 240–262, https://doi.org/10.1016/J.GCA.2013.07.011, 2013.

Taylor, T. N., Taylor, E. L., and Krings, M.: Paleobotany : the biology and evolution of fossil plants, Academic, 2009.

Timm, S., Wittmiß, M., Gamlien, S., Ewald, R., Florian, A., Frank, M., Wirtz, M., Hell, R., Fernie, A. R., and Bauwe, H.: Mitochondrial Dihydrolipoyl Dehydrogenase Activity Shapes Photosynthesis and Photorespiration of Arabidopsis thaliana., The Plant cell, 27, 1968–84, https://doi.org/10.1105/tpc.15.00105, 2015.

Upchurch, Jr, G. R., Kiehl, J., Shields, C., Scherer, J., and Scotese, C.: Latitudinal temperature gradients and high-latitude temperatures during the latest Cretaceous: Congruence of geologic data and climate models, Geology, 43, 683, https://doi.org/10.1130/G36802.1, 2015.

Valdes, P. J., Armstrong, E., Badger, M. P. S., Bradshaw, C. D., Bragg, F., Crucifix, M., Davies-Barnard, T., Day, J. J., Farnsworth, A., Gordon, C., Hopcroft, P. O., Kennedy, A. T., Lord, N. S., Lunt, D. J., Marzocchi, A., Parry, L. M., Pope, V., Roberts, W. H. G., Stone, E. J., Tourte, G. J. L., and Williams, J. H. T.: The BRIDGE HadCM3 family of climate models: HadCM3@Bristol v1.0, Geoscientific Model Development, 10, 3715–3743, https://doi.org/10.5194/gmd-10-3715-2017, 2017.

Van Bodegom, P. M., Douma, J. C., Witte, J. P. M., Ordoñez, J. C., Bartholomeus, R. P., and Aerts, R.: Going beyond limitations of plant functional types when predicting global ecosystem-atmosphere fluxes: exploring the merits of traits-based approaches, Global Ecology and Biogeography, 21, 625–636, https://doi.org/10.1111/j.1466-8238.2011.00717.x, 2012.

Watson, A., Lovelock, J. E., and Margulis, L.: Methanogenesis, fires and the regulation of atmospheric oxygen, Biosystems, 10, 293–298, https://doi.org/10.1016/0303-2647(78)90012-6, 1978.

White, A. A. and Bromley, R. A.: Dynamically consistent, quasi-hydrostatic equations for global models with a complete representation of the Coriolis force, Quarterly Journal of the Royal Meteorological Society, 121, 399–418, https://doi.org/10.1002/qj.49712152208, 1995.

Wildman, R. A., Hickey, L. J., Dickinson, M. B., Berner, R. A., Robinson, J. M., Dietrich, M., Essenhigh, R. H., and Wildman, C. B.: Burning of forest materials under late Paleozoic high atmospheric oxygen levels, Geology, 32, 457, https://doi.org/10.1130/G20255.1, 2004.

Williams, K., Copsey, D., Blockley, E., Bodas-Salcedo, A., Calvert, D., Comer, R., Davis, P., Graham, T., Hewitt, H., Hill, R., et al.: The Met Office global coupled model 3.0 and 3.1 (GC3. 0 and GC3. 1) configurations, Journal of Advances in Modeling Earth Systems, 10, 357–380, 2018.

Wilson, J. P., Montañez, I. P., White, J. D., DiMichele, W. A., McElwain, J. C., Poulsen, C. J., and Hren, M. T.: Dynamic Carboniferous tropical forests: new views of plant function and potential for physiological forcing of climate, New Phytologist, 215, 1333–1353, https://doi.org/10.1111/nph.14700, 2017.

Yu, S., Eder, B., Dennis, R., Chu, S.-H., and Schwartz, S. E.: New unbiased symmetric metrics for evaluation of air quality models, Atmospheric Science Letters, 7, 26–34, https://doi.org/10.1002/asl.125, 2006.